Marine Carbohydrates and Other Sea Spray Aerosol Constituents Across Altitudes in the Lower Troposphere of Ny-Ålesund, Svalbard

Sebastian Zeppenfeld[1]*, Jonas Schaefer[2], Christian Pilz[2], Kerstin Ebell[3], Moritz Zeising[4], Frank Stratmann[2], Holger Siebert[2], Birgit Wehner[2], Matthias Wietz[4,5,6], Astrid Bracher[4,7], and Manuela van Pinxteren[1]

1 Atmospheric Chemistry Department (ACD), Leibniz Institute for Tropospheric Research (TROPOS), Leipzig, Germany
2 Atmospheric Microphysics (AMP), Leibniz Institute for Tropospheric Research (TROPOS), Leipzig, Germany
3 Institute for Geophysics and Meteorology, University of Cologne, Cologne, Germany
4 Alfred Wegener Institute Helmholtz Centre for Polar and Marine Research, Bremerhaven, Germany
5 Max Planck Institute for Marine Microbiology, Bremen, Germany
6 Institute for Chemistry and Biology of the Marine Environment, University of Oldenburg, Oldenburg, Germany
7 Institute of Environmental Physics, University of Bremen, Bremen, Germany

*_Correspondence to_: Sebastian Zeppenfeld (zeppenfeld@tropos.de)

Abstract

Marine combined carbohydrates in aerosol particles ($CCHO_{aer}$) have the potential to influence cloud formation and properties, but it remains unclear to what extent they reach altitudes relevant for cloud processes. Balloon-borne measurements of major sea spray aerosol (SSA) constituents, including sodium (Na^+_{aer}) and $CCHO_{aer}$, were conducted in autumn 2021 and spring 2022 in Ny-Ålesund (Svalbard). Total suspended particles were collected at 321-1112 m, covering both the marine boundary layer and the free troposphere, with Na^+_{aer} ranging 23–850 ng m^{-3} and $CCHO_{aer}$ 3.8–274 ng m^{-3}. The chemical composition of balloon-borne aerosol samples was compared with synchronized ground level measurements at the balloon's winch (Na^+_{aer}: 35–3710 ng m^{-3}; $CCHO_{aer}$: 1.9–194 ng m^{-3}), and at the Old Pier (Na^+_{aer}: 140–1470 ng m^{-3}; $CCHO_{aer}$: 1.6–10.0 ng m^{-3}), where freshly emitted SSA particles were sampled. Surface seawater from the Kongsfjorden was analyzed to evaluate the sea-air transfer of marine CCHO. Air mass histories, atmospheric mixing, and cloud conditions were evaluated for three selected cases to explain vertical concentration patterns. A strong correlation (R=0.78, $p<0.001$) between combined xylose (<0.2–14.1 ng m^{-3}) in $CCHO_{aer}$ and $oxalate_{aer}$ (<1–67 ng m^{-3}) across all altitudes, suggests either coproduction or a connection through atmospheric

processing. These results provide a first comprehensive picture of local primary sea-air transfer of marine combined carbohydrates and highlight the roles of long-range transport, in-situ formation, and atmospheric processing in shaping their distribution.

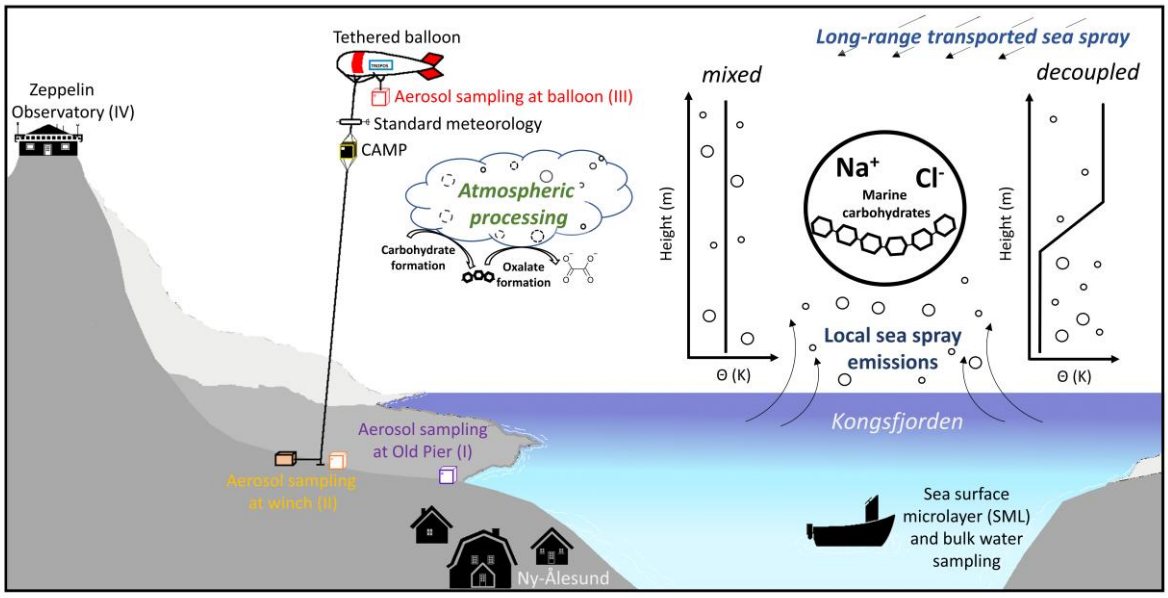

1. Introduction

Aerosol particles in the High Arctic atmosphere originate from a complex interplay of primary and secondary emissions from oceanic, terrestrial, cryospheric, and anthropogenic sources, followed by diverse atmospheric processes (Schmale et al., 2021). They play a crucial role in the radiation balance, directly by scattering and absorbing shortwave and longwave radiation, and indirectly by influencing cloud formation and phase state as cloud condensation nuclei and ice-nucleating particles (Lohmann and Feichter, 2005; Penner et al., 2001; Quinn et al., 2015; Yu et al., 2006). These effects are strongly governed by the particles' size distribution and chemical composition (Dusek et al., 2006; Farmer et al., 2015; Kanji et al., 2017; Pilinis et al., 1995).

The High Arctic predominantly consists of marine areas, characterized by a seasonally variable extent of sea ice cover and open waters. Consequently, sea spray aerosol (SSA) particles represent a key group of primary aerosol particles in this region (Heutte et al., 2025; Kang et al., 2025; Schmale et al., 2022). As Arctic sea ice coverage continues to decline due to global warming, enhanced by Arctic amplification (Cai et al., 2021; Francis and Wu, 2020; Wendisch et al., 2017, 2023), larger expanses of open ocean are anticipated to become significant sources of SSA emissions (Browse et al., 2014; Struthers et al., 2011). Although direct measurements remain sparse, Sharma et al. (2019) readily observed increasing sea salt aerosol production from sea spray over 34 years at the Arctic air chemistry observatory in Alert, Canada.

SSA particles are generated through wind-driven wave action, which causes bubbles at the sea surface to burst, ejecting film and jet droplets into the atmosphere (Veron, 2015). SSA particles primarily consist of inorganic sea salt ions, mainly sodium and chloride, along with organic matter (OM), including significant amounts of marine carbohydrates originating from the sea surface microlayer (SML) and the underlying bulk seawater (Müller et al., 2010; van Pinxteren et al., 2023; Quinn et al., 2015; Russell et al., 2010). In seawater, carbohydrates are produced by photoautotrophic organisms, predominantly as linear or branched oligo- and polysaccharides (Aluwihare et al., 1997; Borch and Kirchman, 1997; Engel and Händel, 2011; Khadem, 2012), collectively referred to as combined carbohydrates (CCHO). They also exist as monosaccharides, known as dissolved free carbohydrates (DFCHO). Both DFCHO and CCHO are consumed or transformed by heterotrophic organisms, with turnover rates largely

determined by the molecular structure and composition of the carbohydrates (Arnosti et al., 2021; Engel and Händel, 2011; Ittekkot et al., 1981; Kirchman et al., 2001).

Sodium in aerosol particles (Na^+_{aer}) is highly abundant in the marine boundary layer, with only minor terrestrial sources and greater atmospheric stability compared to chloride (Cl^-_{aer}) (Chi et al., 2015; Keene et al., 1986; Manders et al., 2010; Sander et al., 2003). This makes it a valuable conservative tracer for studying the sea-to-air transfer and atmospheric transformation of organic compounds, including marine carbohydrates, as well as other inorganic SSA constituents. Notably, the ratio of OM to Na^+ is significantly higher in SSA particles than in seawater, reflecting not only the preferential enrichment of surface-active substances at the interface but also a more complex interplay of factors such as water solubility, biological activity within the ocean surface, and co-adsorption processes involving matrix constituents (Burrows et al., 2014; Gantt et al., 2011; Hasenecz et al., 2020, 2019; Hoffman and Duce, 1976; Jayarathne et al., 2016; van Pinxteren et al., 2017; Quinn et al., 2015; Russell et al., 2010; Schill et al., 2018). This enrichment is particularly pronounced in submicron particles compared to supermicron particles. Furthermore, following the sea-to-air transfer of OM and CCHO, recent laboratory (Hasenecz et al., 2020; Malfatti et al., 2019) and field (Zeppenfeld et al., 2021, 2023) observations suggest their molecular transformation or additional in-situ formation, driven by abiotic, microbial or enzymatic activities in the atmosphere.

SSA particles are known to function as both cloud condensation nuclei (Orellana et al., 2011; Xu et al., 2022) and ice-nucleating particles (Alpert et al., 2022; DeMott et al., 2016; Hill et al., 2023; Mirrielees et al., 2024), underscoring their important role in cloud microphysics, cloud formation, and precipitation processes. Recently, Hartmann et al. (2025) demonstrated, through a combination of lab and field data, that SSA particles' ice-nucleating activity is likely attributable to the polysaccharides they contain. Model simulations further indicated that the ice-nucleating activity of marine polysaccharides is particularly significant within the temperature range between -20 and -15°C in remote oceanic regions, where contributions from terrestrial ice-nucleating particles are minimal or absent. Furthermore, Rocchi et al., (2024) demonstrated that the presence of glucose-rich CCHO, in combination with sea salt, significantly enhances SSA production in eastern Arctic waters. This finding may improve the predictability of SSA emissions in marine models.

In the field, marine combined carbohydrates in aerosol particles ($CCHO_{aer}$) have been predominantly measured at ship-based or coastal locations, which are in close proximity to local marine emission sources both horizontally and vertically (Leck et al., 2013; van Pinxteren et al., 2023; Zeppenfeld et al., 2021, 2023). In contrast, only a few studies have investigated $CCHO_{aer}$ (Karl et al., 2019; Yttri et al., 2024) at an elevated mountain site in a marine-influenced setting, aiming to assess atmospheric concentrations at higher altitudes. Vertically resolved field data comparing ground-level and elevated altitudes using mobile platforms, however, have been unavailable for marine $CCHO_{aer}$ in the past. As a result, it remains unclear to what extent and under which conditions $CCHO_{aer}$ reach the upper marine boundary layer and the free troposphere. This is due to several challenges, including low atmospheric concentrations pushing the instruments' detection capabilities for offline analyses to their limits, the lack of highly resolving online detection techniques for $CCHO_{aer}$, and in particular the absence of lightweight yet powerful pumps with high flow rates. Additionally, the very short sampling times typically available on mobile airborne measurement platforms pose a further obstacle for measuring marine $CCHO_{aer}$ in aerosol particles across altitudes within the troposphere. This lack of vertical field data leaves high uncertainty about the broader relevance of these biomolecules in cloud formation and glaciation beyond a controlled laboratory setup.

Previous airborne measurements around Svalbard (Hara et al., 2003; Simon et al., 2025) and the Canadian Arctic (Köllner et al., 2017) demonstrated that SSA particles, identified by Na^+ and Cl^-, are present in higher altitudes of the lower troposphere, and, to a lesser extent, reach the middle free troposphere (3–6 km a.s.l.). Some of these aerosol particles showed signs of atmospheric aging, such as the replacement of chloride with nitrate and sulfate in the SSA particles. While vertically resolved data exists for major inorganic SSA constituents, such extended information is lacking for marine $CCHO_{aer}$.

Recent methodological advances now allow for a more detailed investigation of the transport mechanisms and atmospheric chemical fate of marine carbohydrates. In this study, we present atmospheric concentrations of these biomolecules alongside common inorganic SSA constituents. Measurements were conducted from ground level up to various altitudes within the boundary layer and lower free troposphere using a tethered helium balloon in Ny-Ålesund on Svalbard during autumn 2021 and spring 2022. For selected cases, we examined the influence of mixing state, meteorological conditions, and air mass history on the observed aerosol composition. Finally, this study addresses the potential atmospheric processing and

transformation of marine carbohydrates, with a focus on their possible contribution to secondary aerosol formation and their implications for atmospheric chemistry and cloud-relevant processes.

2. Experimental

An overview of all analytical and modelling methods applied in this study is provided in **Table 1**.

Table 1. Overview of parameters, methods and sample/media types used in this study.

Category	Parameters	Method/Instrument	Sample/Medium
Major inorganic ions	Na^+, K^+, Mg^{2+}, Ca^{2+}, Cl^-, SO_4^{2-}, oxalate	Ion chromatography	Bulk seawater, SML, aerosol particles (filter)
Free and combined carbohydrates	Fuc, Rha, Ara, Gal, Glc, Xyl, Man, Fru, GalN, GlcN, MurAc, GalAc, GlcAc	HPAEC-PAD	Bulk seawater, SML, aerosol particles (filter)
Sea surface temperature	SST	Digital Thermometer	Ocean surface
Aerosol number concentration	N_{150} (150-2900 nm)	POPS (CAMP)	Atmospheric column
Meteorology	T, U, WD, RH, p, wind, θ, q	Standard meteorology package + thermodynamic equations	Atmosphere at ground (AWIPEV), atmospheric column
Cloud properties	Clouds and hydrometer types, IWP, LWP, IWV	Cloudnet + HATPRO	Atmospheric column
Biogeochemistry (model)	TChl-a, dissolved acidic polysaccharides	FESOM2.1–REcoM3	Ocean surface
Air mass origin	48-h back-trajectories	NOAA HYSPLIT	Several altitudes of atmosphere

2.1 Study area: Ny-Ålesund as an atmospheric observation site

Ny-Ålesund, located at 78.9°N at the Kongsfjorden in Svalbard (Norway), belongs to the world's northernmost permanently inhabited settlements with a year-round accessibility. It serves as a key research site for studying Arctic climate change and Arctic amplification. Ny-Ålesund hosts long-term monitoring sites for aerosols and meteorology, such as the Zeppelin Observatory (Platt et al., 2022), Gruvebadet (Amore et al., 2022), and the AWIPEV Observatory

(Maturilli et al., 2013, 2015). These, along with additional research stations operated by various international institutions, provide valuable data for both long-term atmospheric studies and short-term investigations like the present one.

However, Ny-Ålesund is not representative of the entire High Arctic. Its distinct topography, situated within a fjord and surrounded by high mountains up to 800 m, leads to complex atmospheric dynamics, including foehn-like effects (Shestakova et al., 2021). The local boundary layer is relatively shallow characterized by an average mixing layer height below 700 m and a strong influence by orographic effects (Chang et al., 2017; Dekhtyareva et al., 2018; Gierens et al., 2020). While free-tropospheric winds are predominantly westerly, surface winds result from an interplay of land-sea breeze circulations, southeasterly channeled winds along the fjord axis, and katabatic flows from the Zeppelin mountain range, the Broeggerbreen glacier, or the Kongsvegen glacier (Esau and Repina, 2012; Gierens et al., 2020). Additionally, large wind shear has been observed to generate turbulence, leading to frequent neutral stratification (Gierens et al., 2020). Furthermore, boundary layer mixing can occur even when a positive gradient in potential temperature suggests a more stable stratification. During the present field campaign, we observed that near-surface winds often shift unpredictably, changing direction without a clear pattern, making airflow dynamics challenging to interpret.

From an oceanographic perspective, Svalbard is similarly exceptional. The region is influenced by the cold Arctic waters of the Spitsbergen Polar Current and the warm waters of the West Spitsbergen Current (Feltracco et al., 2021). Kongsfjorden, located on the western coast of Spitsbergen, lies at the interface of High Arctic and Atlantic influences, making it a dynamic and variable environment (Bischof et al., 2019).

Therefore, findings from Ny-Ålesund may not be fully transferable to atmospheric processes over sea ice or the open ocean in the High Arctic. However, in general, the representativeness of any single Arctic site is highly questionable, as Freud et al., (2017) found significant heterogeneity in aerosol particle size distribution across all Arctic sites in their study.

2.2 Field sampling

The field samples (aerosol particles, bulk seawater and SML) for this study were collected near Ny-Ålesund and from the adjacent Kongsfjorden during autumn 2021 and spring 2022.

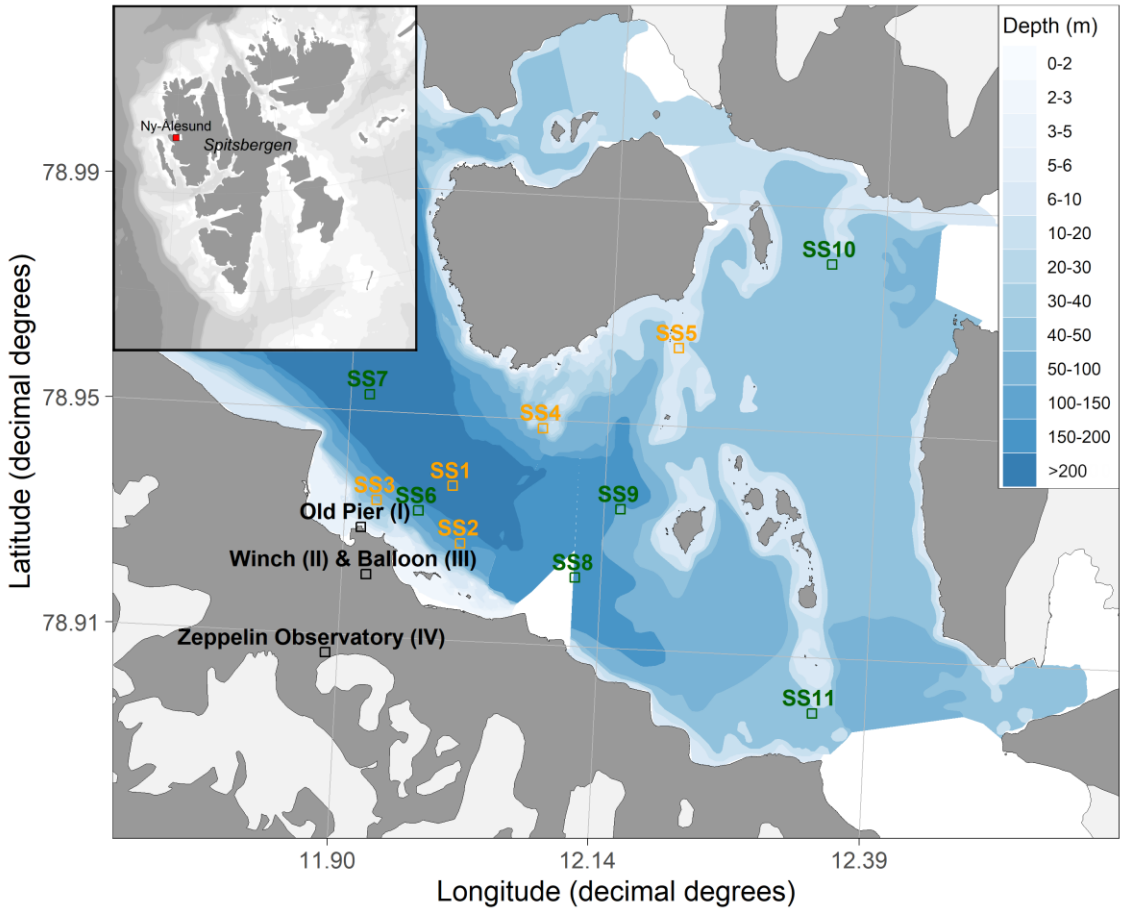

Figure 1. Map of the sampling locations. Aerosol particles were collected at: (I) the Old Pier, representing fresh SSA emissions; (II) the winch, representing ground measurements; (III) the tethered balloon at various altitudes; and (IV) the Zeppelin Observatory, serving as a reference for comparison. Bulk and SML samples were collected from different locations within Kongsfjorden. Orange squares (SS1-SS5) indicate autumn 2021 samples, while green squares (SS6-SS11) represent spring 2022 samples. Blue shading indicates water depth.

a) Bulk seawater and SML sampling

In total, 11 bulk surface seawater and 11 SML samples were taken from a small boat at various dates and locations across the Kongsfjorden (**Figure 1**, **Table S1**). Bulk water samples were obtained from a depth of 1 m using low-density polyethylene (LDPE) bottles secured to a telescopic rod. The corresponding SML samples were collected using the glass plate technique (Cunliffe and Wurl, 2014; van Pinxteren et al., 2012). A glass plate measuring 50 cm × 20 cm × 0.5 cm, with an oval sampling area of 2000 cm^2, was immersed vertically into

188 the surface of the fjord seawater and withdrawn at a steady rate of 15 cm s^{-1}. The SML film
189 attached to the glass surface was drained into a precleaned wide-neck plastic bottle using a
190 funnel and a framed Teflon wiper. Water samples were filtered through 0.2 µm polycarbonate
191 filters (Whatman® Nuclepore™, 47 mm diameter) to separate dissolved and particulate
192 fractions. The filtrate, filters and field blanks were preserved at −20°C until chemical analyses
193 (inorganic ions, carbohydrates). Sea surface temperature (SST) was measured directly from
194 the boat at a depth of approximately 10 cm using a digital thermometer.

195 *b) Aerosol particle sampling in the surroundings of Ny-Ålesund*

196 Total suspended aerosol particles (TSP) were captured on polycarbonate filters (0.8 µm,
197 Whatman® Nuclepore™, 47 mm diameter) at four locations (**Figure 1**): (I) Near the Old Pier
198 next to Kongsfjorden (8 samples), representing fresh SSA emissions; (II) near the balloon winch
199 close to the AWIPEV Observatory (17 samples), representing ground measurements; (III) at
200 high altitudes at the tethered balloon (14 samples); and (IV) at the Zeppelin Observatory
201 (1 sample), serving as a reference for comparison. **Table S2** provides details of individual
202 aerosol particle samplings near the Old Pier (I), while **Table S3** presents the sampling times,
203 locations and heights of all the individual high-altitude aerosol samples (III & IV), along with
204 the corresponding simultaneous ground-level samples (II) taken near the winch.

205 For sampling aerosol particles at the Old Pier (4 m above sea level), a filter holder with a
206 polycarbonate filter attached to a pump was used. Sampling lasted between 4 and 7 days.
207 Flow rates, measured at the beginning and the ending of the sampling with a flowmeter,
208 ranged from 5 to 10 L min^{-1}, with total air volumes between 44 and 82 m^3. The estimated
209 diameter-dependent collection efficiency of this TSP sampling setup, assuming a 90°
210 aspiration angle, is shown in **Figure S1**. To reduce the risk of pump failure due to cold
211 temperatures or snow, the pumps were housed in a Zarges box for protection.

212 High-altitude TSP samples were collected using the helium-filled tethered balloon BELUGA, as
213 described in detail by Pilz et al. (2023). The balloon's altitude was controlled using an electric
214 winch located near the AWIPEV Observatory, with ascent and descent rates from 1 to 3 m s^{-1}.
215 The tethered balloon operated under various meteorological conditions, including both clear
216 and cloudy skies. At a specified altitude, a HALFBAC (High-volume And Light-weight Filter
217 sampler for BAlloon-borne appliCation) (Grawe et al., 2023) collected aerosol particles 2-3 m
218 below the balloon. The HALFBAC is a custom-designed, lightweight aerosol particle sampler

operating at a pump flow between 25 and 35 L min^{-1}. It is capable of collecting sufficient aerosol mass on filters at high altitudes for subsequent offline chemical and microphysical analyses. Simultaneously, another HALFBAC collected ground-level aerosol particles near the electric winch (20 m above sea level). Additionally, one aerosol sample (Filter ID 62, sampling date: 10/05/2022) was collected at the Zeppelin Observatory, a permanent monitoring station located at 474 m a.s.l. on Zeppelinfjellet, using the HALFBAC. Synchronized aerosol particle sampling at the winch and the balloon typically lasted around two hours, as detailed in **Table S3**. The collection efficiency for TSP sampling using HALFBAC is discussed in the supplement (A1) and **Figure S1**.

2.3 Chemical analyses from offline aerosol particle filters and seawater

For the analysis of major cations, anions and marine carbohydrates in aerosol particles, the complete polycarbonate filters were extracted in 6-7 mL of ultrapure water (resistivity > 18.2 MΩ) for two hours followed by a filtration through a 0.45 µm syringe filter. Frozen seawater samples were gently thawed at 4°C one day before analysis.

a) Major cations and anions

Major inorganic ions, including sodium (Na^+), potassium (K^+), magnesium (Mg^{2+}), calcium (Ca^{2+}), chloride (Cl^-), sulfate (SO_4^{2-}), and oxalate, were quantified in 0.45 µm filtered aqueous aerosol extracts, bulk seawater and SML samples using ion chromatography (Dionex ICS-6000, Thermo Scientific) as described by Zeppenfeld et al. (2021). Cations were separated isocratically with a 36 mM methanesulfonic acid eluent on a Dionex IonPac CS16−4 µm column (2 mm × 250 mm), paired with a Dionex IonPac CG16−4 µm guard column (2 mm × 50 mm). For anion separation, a gradient from 4 to 40 mM KOH was applied on a Dionex IonPac AS18 column (2 mm × 250 mm), along with a Dionex IonPac AG18 guard column (2 mm × 50 mm). The analytical uncertainty for each ion was below 5%. Aerosol extracts were measured undiluted, while bulk seawater and SML samples were analyzed at a 1:15,000 dilution.

b) Dissolved free and combined carbohydrates

Carbohydrates in seawater and aerosol particle extracts were measured according to the protocols outlined by Zeppenfeld et al. (2020, 2021), utilizing high-performance anion-exchange chromatography with pulsed amperometric detection (HPAEC-PAD). The system was equipped with a Dionex CarboPac PA20 analytical column (3 mm × 150 mm) and a Dionex CarboPac PA20 guard column (3 mm × 30 mm). The applied eluent gradient separated the following monosaccharide units: fucose (Fuc), rhamnose (Rha), arabinose (Ara), galactose (Gal), glucose (Glc), xylose (Xyl), mannose (Man), fructose (Fru), galactosamine (GalN), glucosamine (GlcN), muramic acid (MurAc), galacturonic acid (GalAc), and glucuronic acid (GlcAc). The analytical uncertainty for each monosaccharide was below 10%. dFCHO represents the total of identifiable free monosaccharides, whereas CCHO include only those monosaccharides released through acid hydrolysis (0.8 M HCl, 100°C, 20 h). For seawater samples, particulate combined carbohydrates (pCCHO, >0.2 µm) were measured from 0.2 µm polycarbonate filters, while dissolved combined carbohydrates (dCCHO, <0.2 µm) were measured from the filtrate after desalination via electrodialysis. Both fractions were later summed to represent the total CCHO. For the winch and balloon samples, the limited air volume and resulting low aerosol mass collected on the filters permitted quantification only of the major monosaccharides (typically Glc, Xyl, Gal, Ara), while minor monosaccharides remained largely below the instrumental detection limits. In contrast, samples from the Old Pier and surface seawater provided sufficient analyte mass to quantify the full suite of the CCHO monosaccharides.

2.4 Vertical profiles from online measurements

a) Size-resolved aerosol particles number concentrations

An optical particles size spectrometer (POPS, Handix), integrated into the Cubic Aerosol Measurement Platform (CAMP) as described by Pilz et al. (2022), provided the integrated total number concentrations (N_{150}) for aerosol particles between 150 and 2900 nm at a temporal resolution of 1 second. On selected dates of HALFBAC sampling, CAMP was operated simultaneously 25 m below the balloon providing insight into the vertical profile of N_{150} during specific events. Vertical profiles are presented as rolling averages over 30 seconds.

b) Meteorological observations and calculations

Standard meteorological parameters, including altitude, ambient temperature (T), wind speed (U), wind direction (WD), air pressure (p), and relative humidity (RH), were measured for the elevated-altitude samples using a standard meteorology package positioned approximately 20 m below the balloon (Pilz et al., 2023). The potential temperature (θ) within the atmospheric column - as a measure of the static stability of the unsaturated atmosphere - was calculated using Eq. I, where T is the ambient temperature (K), p is the atmospheric pressure (hPa), p_0 is the reference pressure (1000 hPa), R is the specific gas constant (287 J kg^{-1} K^{-1}) and c_p is the specific heat capacity of dry air at constant pressure (1004 J kg^{-1} K^{-1}).

$$\theta = \mathrm{T}\left(\frac{p_0}{p}\right)^{\frac{R}{c_p}} \quad \text{(Eq. I)}$$

Specific humidity (q)–remaining constant during adiabatic ascent or descent as long as no phase changes occur–was calculated using Eq. II from Egerer et al. (2021), where R_d/R_v (the ratio of specific gas constants for dry air and water vapor) is approximately 0.622, and $e_s(T)$ represents the temperature-dependent saturation vapor pressure.

$$q = \frac{R_d/R_v \cdot e_S(T) \cdot RH}{p - (1 - R_d/R_v) \cdot e_S(T) \cdot RH} \quad \text{(Eq. II)}$$

Meteorological data measured 2 m above the ground (13 m above sea level) at the AWIPEV Atmospheric Observatory (Maturilli, 2020), represented the weather conditions during aerosol sampling at the winch.

2.5 Supporting observations and model calculations

Major inorganic ions measured at the Zeppelin Observatory with a 24-hour resolution using a statically installed aerosol sampler (Filter_3pack) as part of the European Monitoring and Evaluation Programme (Tørseth et al., 2012) by the Norwegian Polar Institute (NPI) and the Norwegian Institute for Air Research (NILU) were obtained from the EBAS database for the study duration (Aas et al., 2022, 2023). The Filter_3pack data were utilized in two ways:

1. **Comparing sampling techniques:** Data from the Filter_3pack were compared with one HALFBAC aerosol particle sample collected directly at the Zeppelin Observatory (Filter ID 62, 10 May 2022) to evaluate potential artifacts arising from differences in sampling techniques and filter media. Despite variations in time resolution and methods, sodium, potassium, chloride, and sulfate concentrations showed strong agreement (detailed in the supplement A2 and **Figure S2**).
2. **Comparison with balloon data:** Sodium concentrations measured at the Zeppelin Observatory were directly compared with those obtained from the tethered balloon sampling.

Information on the occurrence of clouds and hydrometeor types at Ny-Ålesund were taken from the Cloudnet classification product (Illingworth et al., 2007; Nomokonova et al., 2019), which is based on a combination of ground-based cloud radar, ceilometer, and numerical weather prediction output. Vertically integrated ice water content (IWC), i.e. ice water path (IWP), has been calculated from the Cloudnet IWC product following Hogan et al. (2006). Vertically integrated cloud liquid water (liquid water path; LWP) and water vapor (IWV) were taken from zenith HATPRO microwave radiometer measurements (Nomokonova et al., 2019).

The 48-hour back-trajectories for the aerosol sampling periods were generated using the NOAA HYSPLIT model (Stein et al., 2015). Trajectories were calculated hourly based on GDAS1 meteorological data (Global Data Assimilation System; 1° spatial resolution; 3-hour intervals) for various arrival heights: 50 m (ground level), 474 m (Zeppelin Observatory), and the specific balloon sampling altitudes. Sea ice concentration data were obtained from the NOAA-maintained ERDDAP server (Environmental Research Division's Data Access Program). The back-trajectories were used to assess the relative influence of distant sources, such as the marginal ice zone, versus local ice-free oceanic emissions on the aerosol chemical composition. Given the rather short atmospheric residence time of supermicron SSA particles

(Madry et al., 2011; Veron, 2015), which account for most of the SSA mass in TSP, and the increasing uncertainties associated with longer back-trajectory periods, we considered a 48-hour back-trajectory length appropriate for this analysis.

Ocean surface concentrations for total chlorophyll *a* (TChl-a) and dissolved acidic polysaccharides were obtained by a coupled setup of the ocean sea ice biogeochemistry model FESOM2.1-REcoM3 (Gürses et al., 2023), to which additional state equations have been added to simulate dissolved and particulate organic carbon following Engel et al. (2004) and Schartau et al. (2007). The simulation was set up following Gürses et al. (2023) and using the Arctic-specific tuning of Oziel et al. (2022). Monthly model output was obtained on an irregular grid with approximately 4.5 km resolution in the Arctic Ocean. This configuration has already been applied successfully in Leon-Marcos et al. (2025).

2.6 Statistics, data processing, visualization and text optimization

Statistical analyses, calculations and visualization were conducted using OriginPro 2024, Microsoft Excel, IDL, python3 and R version 4.2.1 with the ncdf4 (Pierce, 2023), openair (Carslaw and Ropkins, 2012), reshape2 (Wickham, 2007), scales (Wickham et al., 2023b), lubridate (Grolemund and Wickham, 2011), cmocean (Thyng et al., 2016), maps (Brownrigg, 2023), mapdata (Brownrigg, 2013), rgdal (Bivand et al., 2022), raster (Hijmans, 2023), RColorBrewer (Neuwirth, 2022), sp (Bivand et al., 2013), dplyr (Wickham et al., 2023a), ggplot2 (Wickham, 2016), and PlotSvalbard (Vihtakari, 2020) packages. Box-and-whisker plots illustrate the interquartile range (box), the median (horizontal line inside the box), the mean (open square), the minimum and maximum values (whiskers). Text and language were optimized using Open AI's ChatGPT-4 Turbo.

3. Results and Discussion

3.1 Chemical constituents in marine aerosol particles from their oceanic source to elevated altitudes

Sodium in aerosol particles (Na^+_{aer})

Sodium, a dominant and chemically stable component of SSA, is commonly used as a tracer for tracking ocean-derived emissions in atmospheric studies (Manders et al., 2010; van Pinxteren et al., 2017; White, 2008). In this study, consistently high Na^+_{aer} concentrations were observed on the TSP filters at the Old Pier next to Kongsfjorden in both autumn 2021 and spring 2022 (**Figure 2a**), ranging from 140 to 1470 ng m^{-3} (median: 495 ng m^{-3}; n=8). The area around Ny-Ålesund, especially the Old Pier, remained largely ice-free, indicating a negligible influence of local sea ice on SSA emissions.

Na^+_{aer} at the winch site, located further inland but still at ground level (35–3710 ng m^{-3}; median: 155 ng m^{-3}; n=17), and at the balloon (321–1112 m; 23–850 ng m^{-3}; median: 124 ng m^{-3}; n=15) was generally lower than at the Old Pier, though episodic high events occurred at all sites. This wide variability from low ng m^{-3} to a few µg m^{-3} agrees with observations from other marine environments and altitudes (Fomba et al., 2014; Li et al., 2024; Ooki et al., 2002; Theodosi et al., 2010; Triesch et al., 2021; Zeppenfeld et al., 2021, 2023).

Since winch and balloon sampling were always synchronized, direct comparisons were possible (**Figure 3**). Several events showed nearly identical Na^+_{aer} concentrations (winch vs. balloon), e.g., 30 Sep: 191 vs. 207 ng m^{-3}; 2 Oct: 35 vs. 36 ng m^{-3}; 9 Oct: 59 vs. 60 ng m^{-3}; 12 Nov: 240 vs. 223 ng m^{-3}. In contrast, other periods exhibited strong vertical gradients with higher ground-level concentrations (e.g., 27 Sep: 1840 vs. 23 ng m^{-3}; 5 Apr: 84 vs. 54 ng m^{-3}; 11 May: 496 vs. 125 ng m^{-3}), while two cases showed higher values at the balloon (24 Sep: 47 vs. 99 ng m^{-3}; 3 Apr: 77 vs. 194 ng m^{-3}). These variations are likely driven by atmospheric processes, including dry and wet deposition (Farmer et al., 2021), dilution during vertical and horizontal transport from the emission region (Wong et al., 2019), vertical mixing (Pilz et al., 2024) and differing air mass histories (Willis et al., 2018), which will be examined in detail for three selected cases later in this study.

Na^+_{aer} at the Zeppelin Observatory largely agreed with the balloon measurements (56–213% overall; 92–107% in five events; **Table S6**), despite differences in time resolution (24 h vs. 1–2 h), sampling altitude, the horizontal distance between the sites, Svalbard's complex topography (Gierens et al., 2020; Shestakova et al., 2021), and the fact that meteorological conditions and atmospheric mixing states have not yet been considered.

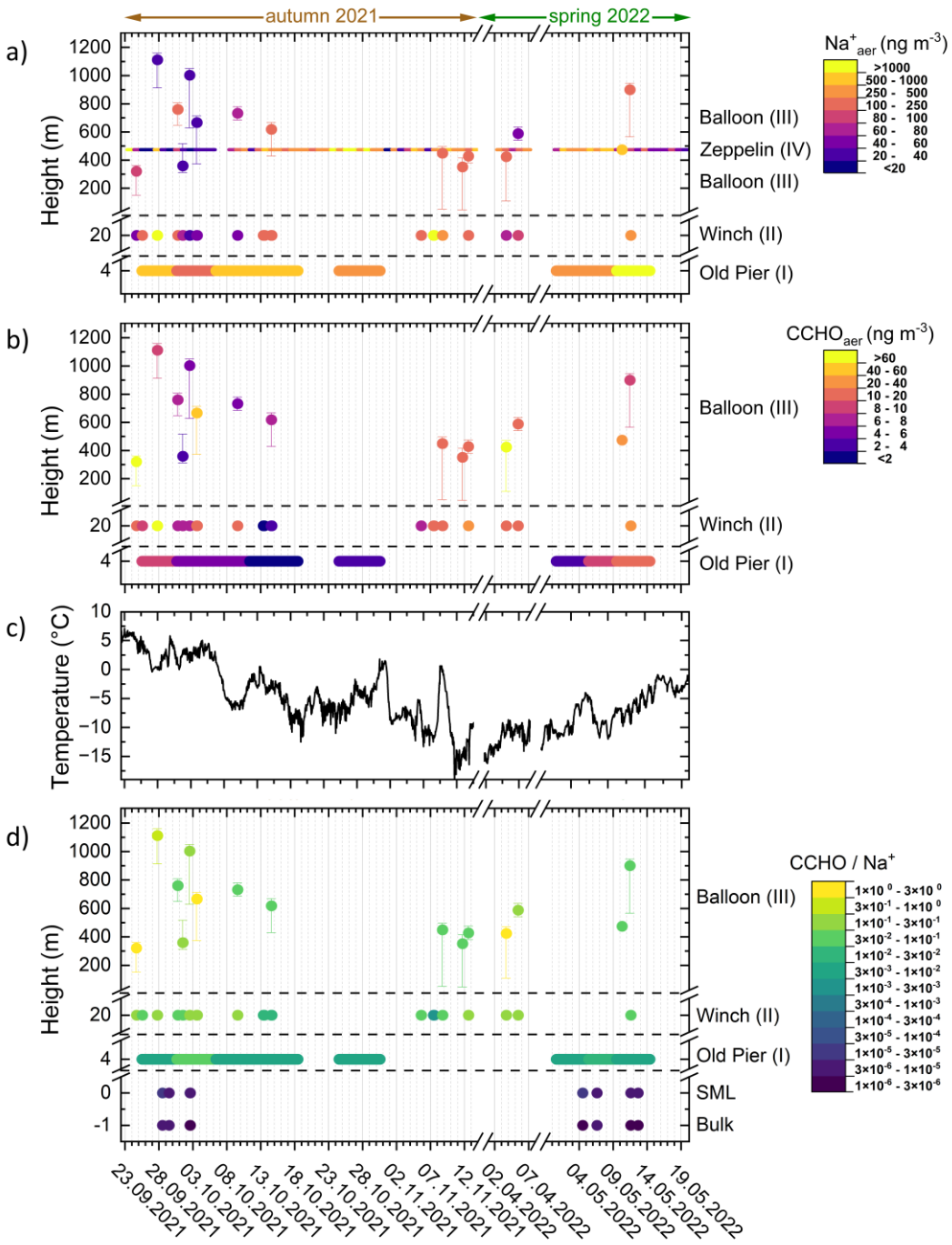

Figure 2. Time-resolved atmospheric concentrations of a) Na^+_{aer} and b) $CCHO_{aer}$ in aerosol particles (TSP) collected in autumn 2021 and spring 2022 in Ny-Ålesund at several heights (m a.s.l.) from four sites: Old Pier, winch near the AWIPEV Observatory, balloon and the Zeppelin Observatory. Dots represent the median height during the total sampling time and vertical error bars represent maximum and minimum height of the sampler during the active sampling. The x-axis ticks represent the start of each date at midnight. c) Air temperature (2 m above ground) measured at the AWIPEV Observatory. d) CCHO/Na^+ ratios within the bulk seawater, the SML and in the aerosol particles at several heights. In panel (a), the label "Balloon (III)" appears twice because balloon sampling for sodium measurements occurred both below and above the fixed altitude of the Zeppelin Observatory.

Overall, Na^+_{aer} was detectable up to 1100 m altitude, sometimes at levels comparable to those near the emission source, indicating effective vertical mixing or transport to cloud-relevant heights via advection. This vertical distribution is consistent with the aircraft-based SSA measurements reported by Hara et al. (2003) and Köllner et al. (2017). Longer atmospheric residence increases the exposure of SSA particles to processing, which can alter their impact on cloud formation. While Na^+_{aer} is considered chemically stable, co-emitted OM including carbohydrates may undergo physical, chemical and microbial changes (Zeppenfeld et al., 2021, 2023). This aspect will be explored further in section 3.3.

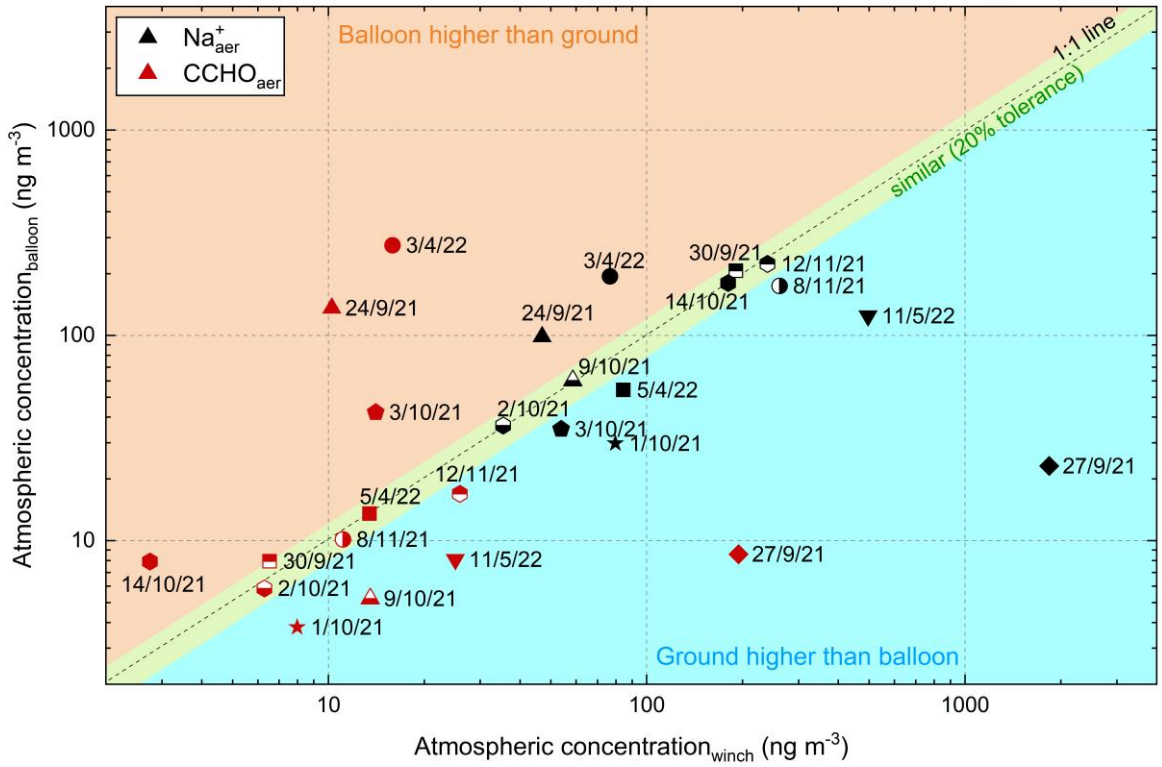

Figure 3. Scatter plot showing Na^+_{aer} (black symbols) and $CCHO_{aer}$ (red symbols) concentrations in TSP measured at the winch, and balloon levels. Data points are categorized to indicate whether values were similar, higher at the balloon, or higher at theground.

Combined carbohydrates in fresh SSA and their oceanic origin

Similar to sodium, $CCHO_{aer}$ were detected at all sites and altitudes (**Figure 2b**). At the Old Pier, $CCHO_{aer}$ concentrations ranged from 1.6 to 10.0 ng m^{-3} (median: 5.0 ng m^{-3}; n=8), showing a seasonal pattern with the highest values at the beginning (end of September 2021) and end (mid of May 2022) of the study, and lower values in October 2021 (**Figure 2c**). No samples were collected between November and April, so winter trends remain unknown.

The seasonal variation of $CCHO_{aer}$ at the Old Pier may be linked to the seasonal dynamics of marine CCHO in the surface water of Kongsfjorden, the only local emission source of SSA. These dynamics are likely driven by seasonal shifts in primary production and phytoplankton composition (Assmy et al., 2023; Mayot et al., 2018, van de Poll et al., 2021).

Similar seasonality was observed for selected monosaccharides among dissolved combined carbohydrates (dCCHO) in Kongsfjorden seawater. In particular, fucose, galactosamine, and rhamnose in bulk water dCCHO exhibited a distinct pattern, closely following SST. Their concentrations peaked in late September/early October, while being much lower (44-67%) in early to mid-May (**Figure 4**). This pattern was weaker for glucose in bulk dCCHO and even less pronounced in the SML for most monosaccharides (**Figure 4**).

In contrast, particulate combined carbohydrates (pCCHO) showed no clear seasonal trend in seawater (**Figure S3**). While dCCHO in bulk water exhibited relatively low spatial and intra-seasonal variability, pCCHO and SML samples were considerably more variable, even among samples from the same season (**Figure S4**). This likely reflects the rapid dynamics of pCCHO's in relation to phytoplankton blooms (Becker et al., 2020; Engel et al., 2012; Fabiano et al., 1993), TEP formation from dCCHO in turbulent waters, and vertical transport of pCCHO through sedimentation (e.g., as marine snow) or its accumulation in the SML depending on buoyancy (Burns et al., 2019; Engel, 2004; Robinson et al., 2019b, a; Wurl and Holmes, 2008). The SML, in particular, may be more sensitive to these dynamics than the bulk water, potentially explaining its greater fluctuations.

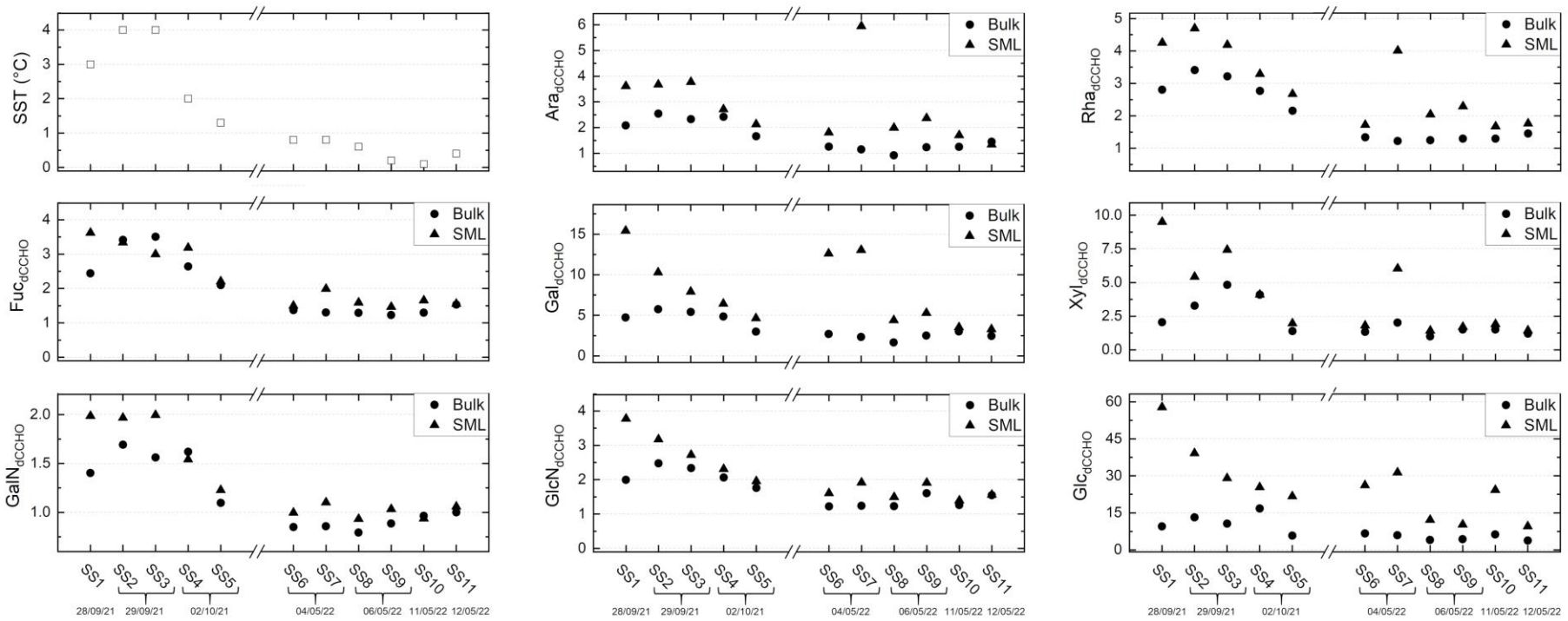

Figure 4. Concentration of measured monosaccharide units in dCCHO from bulk and SML samples collected in Kongsfjorden during autumn 2021 and spring 2022, along with SST measurements taken from bulk samples at the time of sampling.

On the other hand, dCCHO in bulk water, like dissolved organic carbon (Hansell, 2013; Keene et al., 2017), is likely dominated by recalcitrant and semi-recalcitrant compounds, while the labile fraction is rapidly consumed by heterotrophic bacteria (Goldberg et al., 2011). Notably, combined glucose showed high variability in both dCCHO and pCCHO, likely due being the main constituent of abundant storage macromolecules such as laminarin (Becker et al., 2020) during periods of photosynthetic overflow (Barthelmeß et al., 2025), as well as its relatively rapid microbial utilization (Kharbush et al., 2020).

In conclusion, the seasonal variation of $CCHO_{aer}$ aligns with certain marine carbohydrates in Kongsfjorden, suggesting surface dCCHO as the main source of freshly emitted $CCHO_{aer}$.

$CCHO_{aer}$ at the winch and higher altitudes

$CCHO_{aer}$ at the winch site (1.9–194 ng m^{-3}; median: 10.6 ng m^{-3}; n=17) and at the balloon (3.8–274 ng m^{-3}; median: 10.2 ng m^{-3}; n=15), showed broader ranges and significantly higher median and maximum values than at the Old Pier (**Figure 2b**), suggesting sources beyond primary sea-air transfer. Unlike the Old Pier, no clear seasonal pattern or altitude dependence was observed, likely due to the winch site's inland location, making it more sensitive to wind direction and changing weather. Also, the higher temporal resolution of the samples likely captured short-term fluctuations rather than integrated seasonal trends. In addition, atmospheric processing during transport and the lack of true winter samples may have further obscured any clear seasonal signal.

Similar to sodium, some events (**Figure 3**) showed comparable $CCHO_{aer}$ at the winch and balloon (e.g., 30 Sep: 6.5 vs. 8.0 ng m^{-3}; 2 Oct: 6.3 vs. 5.8 ng m^{-3}; 8 Nov: 11.1 vs. 10.2 ng m^{-3}), while on other dates, concentrations were markedly lower at higher altitudes (e.g., 27 Sep: 194 vs. 8.6 ng m^{-3}; 11 May: 25 vs. 8.1 ng m^{-3}), or conversely, higher aloft (e.g., 24 Sep: 10.2 vs. 136 ng m^{-3}; 3 Apr: 15.9 vs. 275 ng m^{-3}). In most cases, $CCHO_{aer}$ covaried with sodium except on 03 Oct, when Na^{+}_{aer} was slightly higher at the ground (54 vs. 35 ng m^{-3})**,** whereas $CCHO_{aer}$ was higher at the balloon (42 ng m^{-3}) than at the winch (14 ng m^{-3}).

To investigate oceanic emission and the atmospheric fate of marine CCHO, CCHO/Na^{+} ratios were calculated for all aerosol, bulk seawater and SML samples, representing the primary sources of the SSA particle constituents studied here (**Figure 2d**). Bulk seawater showed the lowest ratios ($2.0 \times 10^{-6} – 6.0 \times 10^{-6}$) with minimal variability, while the SML had slightly higher

ratios (3.3×10^{-6}–2.5×10^{-5}) due to CCHO enrichment. Specifically, the enrichment factors (EF_{SML}) ranged 1.3 – 4.1 for dCCHO and 0.9 – 6.8 for pCCHO (**Figure S4**), which aligns well with previous studies (Engel and Galgani, 2016; Gao et al., 2012; Zäncker et al., 2021; Zeppenfeld et al., 2021, 2023).

At the Old Pier, where fresh SSA was sampled, the ratios were significantly higher (6.2×10^{-3} – 3.3×10^{-2}) indicating the chemo-selective sea-air transfer that enriches surface-active organics relative to sodium in aerosol particles (Hasenecz et al., 2020, 2019; Jayarathne et al., 2016; Schill et al., 2018; Zeppenfeld et al., 2021, 2023). The enrichment effect is typically more pronounced in submicron particles, which have a higher relative contribution of organics than inorganic ions (Quinn et al., 2015). In contrast, supermicron particles are predominantly composed of sea salts, although organic substances are still notably enriched compared to the surface seawater. As total suspended particles were measured here, and most SSA mass resides in the supermicron range (Facchini et al., 2008; O'Dowd et al., 1997), our results primarily reflect supermicron aerosol composition.

At the winch sampling station, located at ground level but further inland, the CCHO/Na^+ ratios in TSP ranged from 2.9×10^{-3} to 2.6×10^{-1}, similar or slightly higher than at the Old Pier. In contrast, balloon samples from elevated altitudes showed higher ratios ($3.9 \times 10^{-2} – 1.4 \times 10^{0}$), likely due to depletion of salt-rich supermicron particles during dry and wet deposition (Croft et al., 2009; Hoppel et al., 2002; O'Dowd and de Leeuw, 2007), increasing the relative contribution of OM-dominated submicron particles. Furthermore, the increasing absolute concentration of CCHO at higher altitudes (**Figure 2b**) suggests an atmospheric formation process contributing to the elevated CCHO/Na^+ ratios, potentially linked to microbial activity in the atmosphere (see section 3.3). However, because only the major monosaccharides (typically Glc, Xyl, Gal, Ara) could be quantified reliably in the winch and balloon samples, relative CCHO compositions were not assessed across the entire vertical sample set. Therefore, they were not used to further substantiate this conclusion, as it has been done in Zeppenfeld et al. (2021, 2023).

The CCHO/Na^+ ratios observed at the Old Pier and the Winch closely align with ship-based measurements in the High Arctic during the PASCAL cruise (2×10^{-3} to 2×10^{-1} for PM_{10} from summed Berner impactor stages) conducted in May–July 2017 (Zeppenfeld et al., 2023). In contrast, the very high CCHO/Na^+ values ($>1 \times 10^{0}$) observed at some elevated altitudes in this

study were reported only occasionally for submicron particles (0.14–0.42 µm) during PASCAL. This may support the idea that supermicron particle deposition caused the shift in balloon sample ratios, though microbial contributions in the atmosphere are also possible. Moreover, these ratios far exceed those from the Southern Ocean near the western Antarctic Peninsula (8×10^{-4} to 7×10^{-3}) (Zeppenfeld et al., 2021), likely due to differences in surface seawater productivity.

Overall, it can be concluded that both $\mathrm{Na}^{+}_{\mathrm{aer}}$ and $CCHO_{aer}$ are transported from the marine emission source to elevated heights within the lower troposphere. However, with longer atmospheric residence times, the chemical composition of aerosol particles appears increasingly altered in certain samples. As a key factor influencing these observations, the role of meteorological conditions and atmospheric mixing in linking ground and balloon samples will be discussed in the next section.

3.2 Impact of meteorological conditions on SSA particle constituents in higher altitudes

To examine how meteorological conditions and atmospheric mixing influenced Na^{+}_{aer} and $CCHO_{aer}$ at elevated altitudes, three distinct cases with distinct, unvarying constant weather conditions were selected (**Figure 5**). These conditions allow for a detailed interpretation of the observed chemical values.

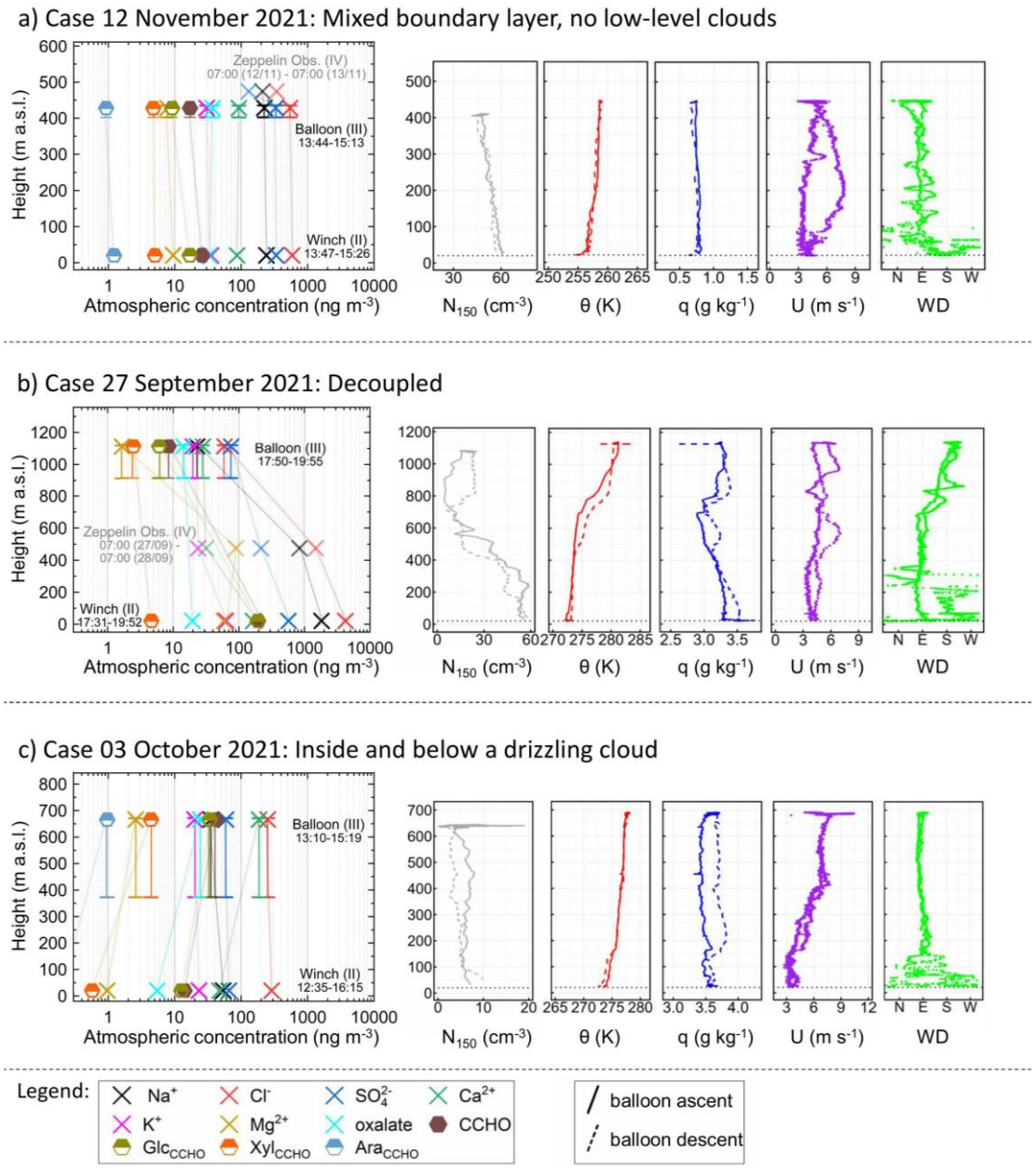

Figure 5. Vertical profiles of three atmospheric cases showing mass concentrations of chemical constituents (inorganic ions, oxalate, total $CCHO_{aer}$, and major monosaccharides within $CCHO_{aer}$) in aerosol particles, measured on the ground (winch) and aloft (balloon) using offline filters. Vertical error bars indicate the range between minimal and maximal heights during active sampling at the balloon, while the symbols denote the median sampling heights. Data from the Zeppelin Observatory are also included when available and above detection limits, albeit with a 24-hour resolution. Dotted lines are included to aid in reading the vertical distribution of individual chemical substances. These profiles are complemented by aerosol particle number concentrations of particles bigger than 150 nm (N_{150}), potential temperature (θ), specific humidity (q), wind speed (U), and wind direction (WD) measured during the ascents (solid lines) and descents (dashed lines) of the balloon.

To assess atmospheric stability and layering in these cases, vertical profiles of potential temperature were utilized. To further confirm aerosol mixing conditions, additional meteorological parameters (specific humidity, wind speed and direction), vertical aerosol particle number concentrations of particles larger than 150 nm (N_{150}) (**Figure 5**), cloud conditions (**Figure S5**) and back-trajectory analyses (**Figure 6**) were considered. The selected cases include (a) a cloud-free mixed boundary layer (12 Nov 2021), (b) a free troposphere decoupled from the ground (27 Sep 2021), and (c) a boundary layer capped by precipitating clouds (03 Oct 2021).

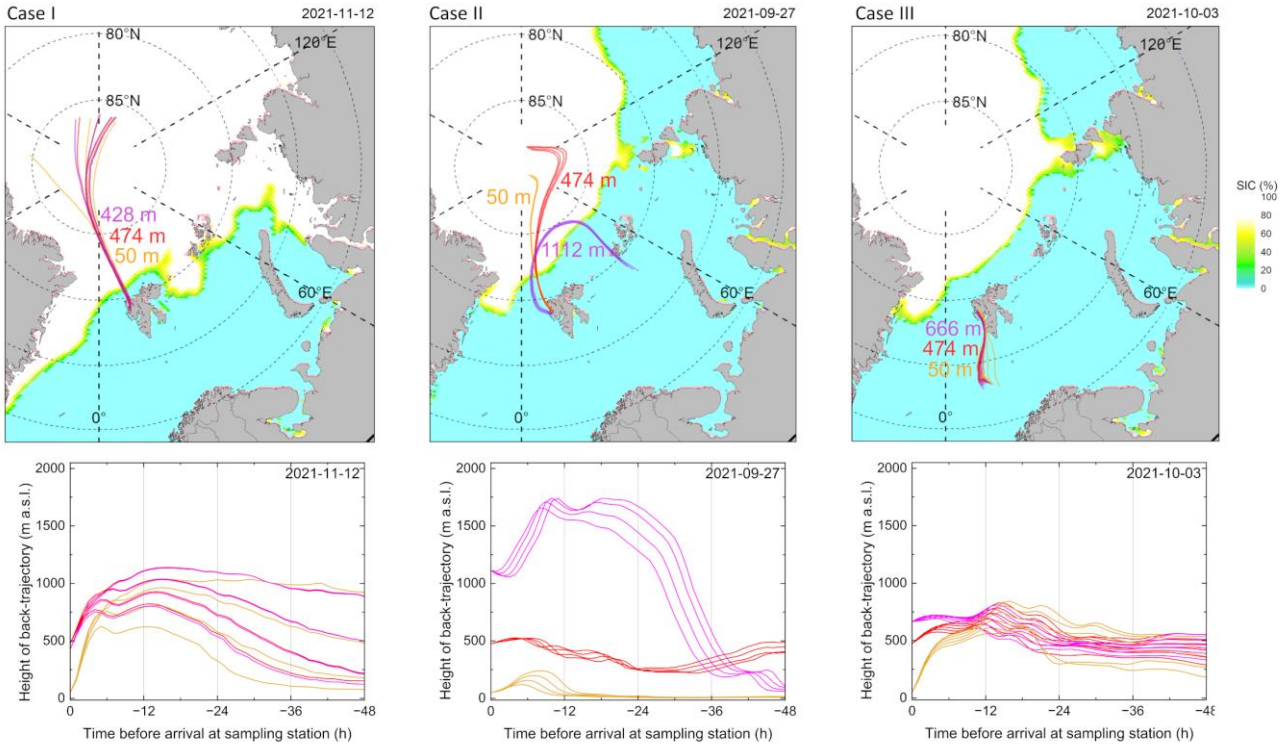

Figure 6. 48-hour back-trajectories calculated on an hourly basis for three arrival heights: orange (50 m, ground-level air masses), red (474 m, height of the Zeppelin Observatory), and purple (variable arrival height, high-altitude air masses sampled at tethered balloon). These are accompanied by daily sea ice concentration (SIC) maps (top) and height profiles (bottom) for three selected aerosol particle sampling cases.

Case I: Mixed boundary layer & no low-level clouds

On 12 November 2021, during the polar night, two HALFBACs were operated simultaneously at the ground and the balloon (median altitude of 428 m) for approximately 90 min. Ground-level conditions were −16.7°C, 69% RH, and 1.5 m s^{-1} wind mainly from the southwest. At the balloon, sampling occurred at a similar temperature (−17.5°C) and RH (72%), but higher wind speeds (4.3 m s^{-1}) from the northeast to southeast. With IWV < 3 kg m^{-2}, the atmosphere was very dry (**Figure S5a**), and only a thin mixed-phase cloud layer at 4.5–5 km altitude was

present, with negligible LWP and IWP (**Figure S5a**), unlikely to affect aerosol chemistry within the boundary layer.

During the balloon's ascent, potential temperature increased from 255 K to 258 K, with the strongest gradient near the ground. Using the wind speed profile and the Richardson number approach (Akansu et al., 2023), a very shallow surface mixing layer of ~12 m was estimated, likely caused by recent surface cooling. Although this surface inversion and the slightly stable to near-neutral stratification above would limit instantaneous vertical mixing, surface mixing layer height reflects only momentary conditions, whereas aerosol and humidity profiles integrate mixing over longer timescales. The coupling state at the time of measurement is therefore not a reliable indicator of the effective boundary-layer mixing state. Furthermore, as noted in Section 2.1, Ny-Ålesund's complex orography can induce localized turbulent mixing even under stable stratification. In addition, a low-level jet observed during descent, with wind speeds at least 2 m s^{-1} higher than above and below, provided a significant additional source of turbulence and vertical mixing within the boundary layer (Egerer et al., 2023).

At the ground, N_{150} was around 60 cm^{-3}, and gradually decreased to 45 cm^{-3} at the balloon's sampling height, indicating a fairly uniform aerosol distribution dominated by primary emissions. Combined with nearly constant specific humidity (~0.7–0.8 g kg^{-1}), a slight wind speed increase with altitude, the low-level jet during descent, and consistent wind direction (**Figure 4a**), these suggest a largely well-mixed boundary layer. HALFBAC samples from ground and balloon showed similar concentrations of inorganic ions (Na^+_{aer}: 240 & 223, Cl^-_{aer}: 586 & 543, $SO^{2-}_{4\,aer}$: 336 & 330, Ca^{2+}_{aer}: 87 & 92, Mg^{2+}_{aer}: 9.5 & 7.8, K^+_{aer}: 34 & 30 ng m^{-3}), $oxalate_{aer}$ (34 & 37 ng m^{-3}), and major CCHO-bound monosaccharides ($Glc_{CCHO,aer}$: 17 & 9.1, $Xyl_{CCHO,aer}$: 5.0 & 4.7, $Ara_{CCHO,aer}$: 1.2 & 0.9 ng m^{-3}), supporting a well-mixed layer. Despite diverse sources (SSA, dust, anthropogenic, secondary), vertical aerosol composition remained uniform. Zeppelin Observatory 24 h measurements of Na^+_{aer}, Cl^-_{aer}, and SO^{2-}_4showed slightly lower concentrations but agreed with balloon results.

Back-trajectory analysis revealed that air masses at ground level, the balloon, and Zeppelin Observatory (**Figure 6, Case I**) followed the same path during the 48 hours before sampling. Originating from the Arctic pack ice, they crossed the marginal ice zone with a short residence time before passing over the ice-free ocean and Kongsfjorden, where most SSA compounds were likely taken up. The back-trajectory heights indicate a vertical connection between the

three air masses, confirming a similar transport history, influenced by the same emission sources.

This case demonstrates that major SSA constituents (Na^+_{aer}, Cl^-_{aer}, and $CCHO_{aer}$) can mix effectively within the boundary layer, reaching altitudes relevant to cloud formation with concentrations nearly identical to ground level, and that such a mixing state can persist during temporarily decoupled conditions, provided there is no additional aerosol particle source at the ground or aloft.

Case II: Free troposphere decoupled from the ground

On 27 September 2021, balloon measurements were conducted at a median altitude of 1112 m, above both the Zeppelin Observatory and the altitude range of Case I, i.e. in the free troposphere above the boundary layer. A strong increase of the potential temperature between 700 m (θ≈274 K) and 900 m (θ≈280 K) indicates a pronounced inversion (**Figure 5b**). N_{150} peaked near the ground, remained stable in the lowest 200 m, decreased up to ~700 m, and slightly increased toward 1112 m, suggesting sources other than the ground. Specific humidity varied strongly (2.6–4 g kg^{-1}), confirming a decoupled atmospheric layer.

During ground sampling, mean conditions were 3 °C, 89 % RH, and 0.7 m s^{-1} wind from the southwest (**Table S5**). At balloon altitude, air was colder (−1.9 °C), slightly drier (87 % RH), and much windier (5.5 m s^{-1}), primarily from the south and southwest (**Table S4**). IWV increased from 13 to ~15 kg m^{-2} during sampling (**Figure S5b**). A dense warm-front cloud layer (2–8 km) with mainly cloud ice (IWP up to 1.4 kg m^{-2}) was present (**Figure S5b**). Precipitation reached the balloon as snowfall only in the last 15–30 min of sampling.

On this date, we observed a strong vertical gradient in both $\mathrm{Na}^+_{\mathrm{aer}}$ and $CCHO_{aer}$ concentrations (**Figure 5b**), starting from the winch ($\mathrm{Na}^+_{\mathrm{aer}}$: 1840 ng m^{-3}, $CCHO_{aer}$: 199 ng m^{-3}), decreasing at the Zeppelin Observatory ($\mathrm{Na}^+_{\mathrm{aer}}$: 850 ng m^{-3}), and dropping sharply at the balloon's altitude ($\mathrm{Na}^+_{\mathrm{aer}}$: 23 ng m^{-3}, $CCHO_{aer}$: 8.6 ng m^{-3}). Similar declines occurred for $\mathrm{SO}^{2-}_{4\,\mathrm{aer}}$ (580; 220; 76 ng m^{-3}), $\mathrm{Cl}^-_{\mathrm{aer}}$ (4230; 1500; 60 ng m^{-3}), and $\mathrm{Ca}^{2+}_{\mathrm{aer}}$ (165; 32; 28 ng m^{-3}). This pronounced decrease with altitude indicates separation between ground-level and elevated air masses, making fresh local SSA from Kongsfjorden or the west coast of Svalbard an unlikely source for the substances detected at 1112 m.

This assumption is supported by back-trajectory analysis (**Figure 6b**): air masses at 50 m and 474 m arrival height originated from Arctic pack ice and crossed the ice-free Fram Strait, whereas the 1112 m air mass followed a different path over the Barents Sea near Franz Josef Land. After contact with the marine boundary layer and possibly the sea surface about 48 h before sampling, it remained mainly between 1000 and 1800 m. This indicates that the SSA observed at 1112 m in Ny-Ålesund likely originated from this distant source region.

In summary, Case II demonstrates that major SSA constituents (Na^{+}_{aer}, Ca^{2+}_{aer}, Cl^{-}_{aer}, $SO^{2-}_{4\,aer}$ and $CCHO_{aer}$) can be present in the free troposphere and likely originate from a distant source. However, they appear at different concentrations above the temperature inversion than in the mixed boundary layer below, where concentrations, like in Case I, are similar.

Case III: Inside and below a drizzling cloud

On 03 October 2021, the ground temperature was 3°C with a high relative humidity of 89%. Winds were light, shifting between east, south, and west at 0.7 m s^{-1} during sampling. At the balloon's altitude of 666 m, the average temperature was -1.3°C, the relative humidity 96% and the wind speed 6.8 m s^{-1} from the east and northeast. The day was overcast, with continuous drizzle from a 2 km deep mixed-phase cloud layer with LWP values of up to 300 g m^{-2} and IWV of around 13 to 14 kg m^{-2}. The balloon's altitude was close to the melting layer.

During the balloon's ascent and descent to 666 m, a positive gradient in potential temperature (272 K at the ground vs. 278 K at the balloon, **Figure 5c**) indicated a stably stratified boundary layer. Specific humidity was uniform (3.2–3.8 g kg^{-1}), while N_{150} was lower than in Case I (3–10 cm^{-3}) with higher relative variability, likely influenced by low counting statistics at these low concentrations. Overall, mixing conditions in Case III were similar to Case I, but sampling occurred partly within or below a drizzling low-level cloud.

Back-trajectory analysis (**Figure 6, Case III**) showed that air masses at the altitudes of ground, balloon, and Zeppelin Observatory followed the same 48-h path from the ice-free ocean south of Svalbard. Vertical trajectory heights indicate shared transport history and influence by the same emission sources, consistent with Case I.

In line with the lower aerosol number concentrations, offline measurements of chemical constituents were also generally lower than in the previous cases. Furthermore, major inorganic ions (**Figure 5c**) were generally similar at the ground and balloon (Cl^{-}_{aer}: 289 &

252 ng m^{-3}; $SO_{4\,aer}^{2-}$: 66 & 59 ng m^{-3}; K_{aer}^{+}: 23 & 20 ng m^{-3}), with Na_{aer}^{+} (53 & 35 ng m^{-3}) somewhat higher at the ground. At the Zeppelin Observatory, only Na_{aer}^{+} exceeded the detection limit, with a concentration of 38 ng m^{-3}, very similar to the value observed at the balloon. This consistency indicates a rather mixed boundary layer. Creamean et al. (2021) analyzed three years of Arctic aerosol vertical distributions using a tethered balloon in Alaska and found that, when a uniform aerosol distribution below clouds was observed, it primarily occurred in autumn, aligning well with Case III.

Interestingly, despite the same levels of major inorganic ions, some chemical constituents exhibited increased concentrations at higher altitudes. These included major monosaccharides bound within CCHO (ground & balloon: $Glc_{CCHO,aer}$: 12.6 & 34 ng m^{-3}; $Xyl_{CCHO,aer}$: 0.57 & 4.4 ng m^{-3}; $Ara_{CCHO,aer}$: below detection limit & 0.97 ng m^{-3}), as well as $oxalate_{aer}$ (5.5 & 24 ng m^{-3}), Ca_{aer}^{2+}(47 & 187 ng m^{-3}), and Mg_{aer}^{2+} (0.97 & 2.6 ng m^{-3}). These elevated concentrations cannot be explained by direct local sea spray emissions or remote source contributions alone, suggesting the involvement of cloud-related enrichment and transformation processes.

Soluble Ca_{aer}^{2+} and Mg_{aer}^{2+} possibly derived from preexisting organic structures in SSA, becoming soluble and detectable after chemical aging. OM-bound Ca^{2+}, as already found in Antarctic SSA (Su et al., 2023), may originate from SML-derived polysaccharide gels such as TEPs, and airborne algal cells or fragments, which can release Ca^{2+} and Mg^{2+} through gel dispersion or cell dissolution under the acidic conditions of chemically aged SSA aerosol particles (Aller et al., 2017; Angle et al., 2021; Orellana and Leck, 2015; van Pinxteren et al., 2022; Trainic et al., 2018; Zhu et al., 2014). Since these particles were sampled in cloud water, which contains abundant TEP (van Pinxteren et al., 2022), this mechanism may also explain the elevated CCHO concentrations. Ca_{aer}^{2+} can form complexes with $oxalate_{aer}$ (Furukawa and Takahashi, 2011), and oxalic acid increases hygroscopicity, potentially accounting for the high values observed at the balloon in Case III. In addition, secondary in-situ atmospheric or microbial origins, particularly in the aqueous phase, may contribute to $CCHO_{aer}$ and $oxalate_{aer}$ and is discussed in the following section.

In summary, Case III demonstrates that certain SSA constituents can vary with altitude due to atmospheric processing following primary emissions and vertical transport.

665 The three cases show that meteorological conditions can produce similar, lower, or higher
666 chemical concentrations at different altitudes. Porter et al. (2022) observed similar patterns
667 for ice-nucleating particles at the North Pole. They combined their measurements with
668 trajectory analyses and heat sensitivity tests to conclude on aerosol sources. While this effect-
669 based approach gives insights into particle properties, direct chemical analyses, as performed
670 in this study, can further enhance certainty about particle origin and composition relevant for
671 cloud formation.

3.3 Factors affecting SSA constituents beyond local sea-air transfer

Long-range transport and size-dependent deposition

SSA particles originate from both local and remote marine regions. However, our sampling methods make it challenging to determine the relative contribution of long-range transported SSA constituents, particularly when a local marine source, such as the Kongsfjorden is adjacent to the sampling site and may dominate other marine emissions.

As demonstrated in Case II, long-range transport of SSA can become dominant when air masses at elevated altitudes are decoupled from those at the ground. In this case, vertical and horizontal trajectory analysis suggests that the measured SSA constituents may have been emitted and incorporated into the atmosphere approximately 48 hours earlier over the Barents Sea, near Franz Josef Land. Typical removal processes of supermicron particles, such as dry and wet deposition or cloud droplet activation, likely reduced the atmospheric concentrations of major inorganic ions and $CCHO_{aer}$ by one to two orders of magnitude before the arrival of the air masses in Ny-Ålesund (**Figure 5b**).

In several balloon-borne TSP filter samples, an elevated $CCHO_{aer}/Na^{+}_{aer}$ ratio was observed, most notably on 24 Sep 2021; 03 Oct 2021 (Case III) and 03 Apr 2022 (see **Figure 2d**). These values far exceeded both ground-based aerosol measurements from this study and previously reported values (Zeppenfeld et al., 2021, 2023), particularly for supermicron SSA particles that dominate the TSP mass. A slight increase of this ratio may be explained by a longer atmospheric residence time of these particles. This leads to a relative reduction of supermicron aerosol particles, typically dominated by sea salt (O'Dowd and de Leeuw, 2007), through deposition (Croft et al., 2009; Hoppel et al., 2002). In contrast, submicron aerosol particles, which are rich in surface-active CCHO, remain. This process could lead to a shift of the $CCHO_{aer}/Na^{+}_{aer}$ ratios more characteristic of submicron than supermicron particles in the TSP samples of this study, as seen in Case II.

However, for the three cases with the most pronounced increases in $CCHO_{aer}/Na^{+}_{aer}$ ratios in TSP at higher altitudes (24 Sep 2021; 03 Oct 2021; 03 Apr 2022), absolute $CCHO_{aer}$ concentrations were also elevated (compare **Figures 2b and 2d**). Such increases in absolute concentrations cannot be explained by the selective removal of supermicron particles as hypothesized above. This raises the question of whether the observed $CCHO_{aer}$ concentrations

could result from the long-range transport of SSA compounds from a distant marine source with significantly higher CCHO levels than the local Kongsfjorden.

Model simulations using FESOM2.1-REcoM3 (Gürses et al., 2023) (**Figure S6**) and field data (Assmy et al., 2023; Feltracco et al., 2021; Grosse et al., 2021; Wietz et al., 2024) confirm that the eastern Fram Strait as well as coastal Svalbard waters are productive and polysaccharide-rich regions. While the FESOM2.1-REcoM3 model does not resolve the SML separately, previous studies have shown significant CCHO enrichment in this layer (Compiano et al., 1993; Engel and Galgani, 2016; Gao et al., 2012; Zäncker et al., 2021), particularly in the productive marginal ice zone (Zeppenfeld et al., 2023). However, in cases of high $CCHO_{aer}$ at higher altitudes in this study, air mass trajectories did not pass over any of these productive marine regions within 48 hours before reaching Svalbard (**Figure S7**). These findings suggest that long-range transport of SSA from more productive remote marine sources is unlikely to explain the elevated $CCHO_{aer}$ concentrations at elevated altitudes within the lower troposphere in Ny-Ålesund, further supporting a predominantly local source or atmospheric in-situ formation.

In summary, while long-range transport of SSA constituents at elevated altitudes appears relevant in cases of decoupled atmospheric layers such as in Case II, it may not explain the significantly higher $CCHO_{aer}$ concentrations at high altitudes compared to ground levels. Instead, in-situ formation of $CCHO_{aer}$ could be a more plausible explanation for these observations.

Atmospheric in-situ formation of marine $CCHO_{aer}$

Bacteria can be transported into and persist in the Arctic atmosphere (Jensen et al., 2022; Šantl-Temkiv et al., 2018), with sources including terrestrial environments and surface seawater, particularly the SML (Aller et al., 2005). Our complementary microbiological sampling during our campaign supported such dynamics by detecting diverse marine bacteria in aerosol particles (Wietz et al., 2025). Some aerosolized taxa, for instance *Polaribacter*, encode multiple genes for CCHO metabolism (Avcı et al., 2020) and consistently occur in both Kongsfjorden seawater and atmosphere during the spring bloom (Feltracco et al., 2021). These observations might underpin microbial CCHO transformations in the atmosphere, for instance the production of polysaccharide-based gels as protection against temperature fluctuations, salinity changes, and desiccation (Aller et al., 2005; Ramasamy et al., 2023; Šantl-Temkiv et al.,

2022). Under highly humid conditions, especially in the presence of liquid water (such as in Case III), airborne bacteria can become metabolically active (Ervens and Amato, 2020; Haddrell and Thomas, 2017). Atmospheric OM formation, including CCHO, through microbial activity has been documented for cloud water and aerosol particles (Bianco et al., 2019; Klein et al., 2016; Matulová et al., 2014). Consequently, metabolically active bacteria in the atmosphere could explain the increased $CCHO_{aer}$ concentrations observed within or near drizzling clouds in Case III of this study.

$CCHO_{aer}$ versus $oxalate_{aer}$: Co-production or atmospheric processing?

Since both combined glucose and combined xylose were consistently detected in $CCHO_{aer}$ of nearly all aerosol samples, we examined their correlation with other atmospheric chemical parameters. We observed a strong correlation between atmospheric xylose in $CCHO_{aer}$ and $oxalate_{aer}$ with an R=0.78 ($p<0.001$) across all sampling locations and heights (**Figure 7**). Oxalate, the ionic form of oxalic acid, is the most abundant dicarboxylic acid in aerosol particles (Kerminen et al., 1999; Rinaldi et al., 2011), with atmospheric concentrations in this study between <1 and 67 ng m^{-3}. The strong correlation raised the question of whether oxalic acid could be chemically linked to combined carbohydrates in aerosol particles.

$Oxalate_{aer}$ is known to originate from several primary sources and secondary formation pathways in both terrestrial and anthropogenic environments (Kawamura and Bikkina, 2016; Yang et al., 2022). In remote marine environments, the atmospheric formation of oxalic acid was proposed by Warneck (2003) through the aqueous-phase oxidation of glyoxal and glycolaldehyde, a process also investigated by field measurements inside and above marine clouds (Crahan et al., 2004; Sorooshian et al., 2007) and modeling (Herrmann et al., 2005; Tilgner and Herrmann, 2010). The possible aqueous-phase formation was supported by Case III of this study, where higher $oxalate_{aer}$ concentrations were observed within and in vicinity of clouds compared to ground level. In contrast, in the drier conditions of Cases I and II, $oxalate_{aer}$ levels remained vertically uniform. Additionally, since overall $oxalate_{aer}$ levels at the Old Pier (1.1–10.1 ng m^{-3}; mean=4.3±3.5 ng m^{-3}) were relatively low compared to the more inland Winch (<1–58 ng m^{-3}; mean=19.8±16.2 ng m^{-3}) and elevated altitudes samples (4.6–67 ng m^{-3}; mean=29.6±17.8 ng m^{-3}), direct primary oceanic emission was likely not its dominant source.

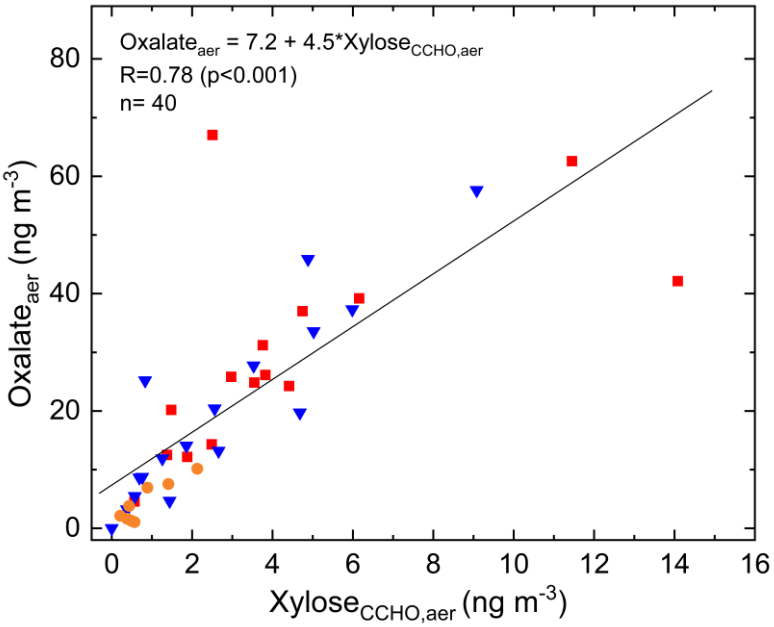

Figure 7. Atmospheric oxalate as a function of xylose in $CCHO_{aer}$ (R=0.78; p<0.001) measured in TSP from the Old Pier (orange circles), the winch site (blue triangles) and at elevated altitudes (red squares).

But what are the precursors of oxalic acid's precursors? While Warneck (2003) suggested that the anthropogenic volatile organic compounds acetylene and ethene can be transformed to atmospheric glyoxal, other studies suggest the photochemical degradation of marine OM (McNeill, 2015; Sinreich et al., 2010; Turekian et al., 2003; Zhou et al., 2014), with oligo- and polysaccharides representing a known subclass. Although not explicitly measured in this study, previous findings have shown that both $CCHO_{aer}$ (Leck et al., 2013; Zeppenfeld et al., 2021, 2023) and $oxalate_{aer}$ (Guo et al., 2016; Rinaldi et al., 2011; Turekian et al., 2003) are present across both the accumulation and coarse size modes. However, no consistently dominant size mode has been identified, which may support a common mechanism of formation or similar atmospheric processing pathways.

Here, based on known chemical reactions, we propose possible atmospheric pathways linking xylose-containing oligo-and polysaccharides as the precursors to oxalate as the final product (**Figure 8**). The initial depolymerization of CCHO presumably occurs either via enzymatic degradation, e.g. by glycoside hydrolases, or acid hydrolysis (Panagiotopoulos and Sempéré, 2005), both of which are plausible in the atmospheric context. Active microbial enzymes have been detected in SSA, often exhibiting activities 1–2 orders of magnitude higher than in bulk seawater (Malfatti et al., 2019). Additionally, SSA particles are known for reaching very low pH

levels within minutes after their emissions due to the uptake and reactions with acidic gases, as well as water loss (Angle et al., 2022, 2021). Furthermore, although not explicitly investigated in an atmospheric context, Zhu et al. (2023) observed rapid depolymerization of xylose-containing oligosaccharides into the monosaccharide xylose within minutes in a UV/H_2O_2 system, which generates hydroxyl radicals.

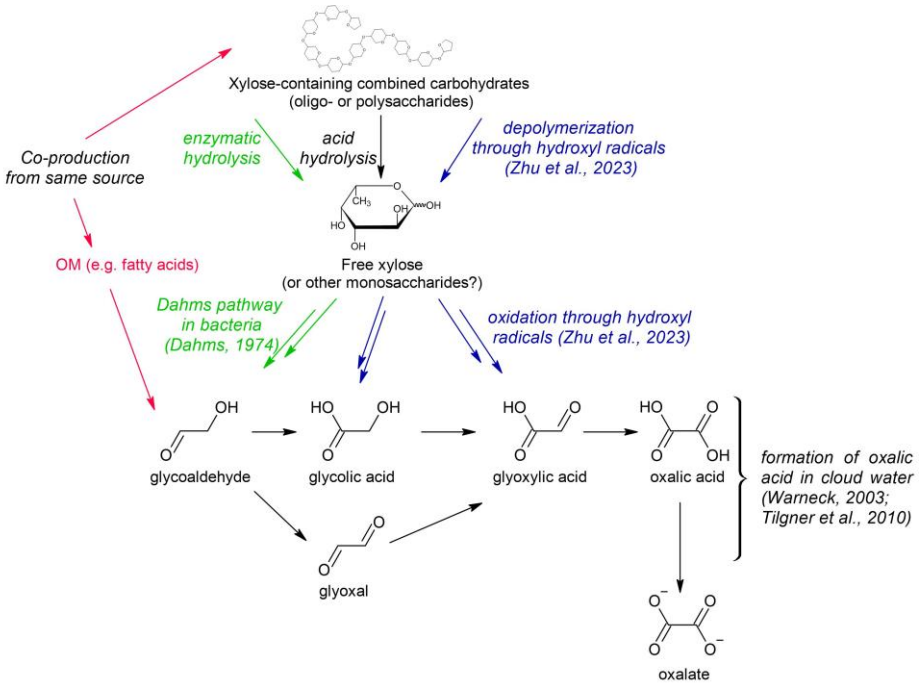

Figure 8. Possible pathways for the formation of atmospheric oxalate from xylose in combined carbohydrates in marine aerosol particles.

With one exception, free xylose was never detected in any aerosol sample of this study. This suggests two possible explanations. First, xylose may have remained bound within the $CCHO_{aer}$ fraction and was not released into its free form. In this case, it would indicate co-emission without a chemical pathway leading to oxalate. Second, free xylose may have been rapidly processed in the atmosphere via reactions described below.

Two potential pathways may link monomeric xylose to precursors of Warneck's oxalate formation: (1) a follow-up reaction with hydroxyl radicals, where the pyranose ring of xylose is cleaved after the more susceptible glycosidic bonds have been readily broken. Zhu et al. (2023) observed glycolic acid and glyoxylic acid among other products following the UV/H_2O_2 treatment of xylooligosaccharides. (2) Bacterial metabolism via the Dahms pathway converting free xylose into pyruvate and glycolaldehyde (Dahms, 1974). However, only few

bacteria encode this pathway; and it is highly questionable whether these occur in sufficient atmospheric concentrations for a measurable effect.

One indication that direct formation from xylose-containing oligo- and polysaccharides cannot be the sole source of atmospheric oxalate in the marine environment is the discrepancy in concentrations: atmospheric oxalate levels were seven times higher than those of combined xylose. This confirms the involvement of additional precursors or a co-production/co-emission of combined xylose with gaseous precursors, such as isoprene (Carlton et al., 2009; Kawamura and Bikkina, 2016), or other primary marine organic matter, such as phytoplankton-derived fatty acids (Kawamura et al., 1996b, a) undergoing photo-oxidation. Further targeted laboratory and modeling studies are needed for clarity.

4. Summary and Atmospheric Implications

In autumn 2021 and spring 2022, we performed balloon-borne measurements of major SSA constituents at Ny-Ålesund (Svalbard). Our evidence demonstrated that both sodium and marine CCHO reach elevated altitudes within the boundary layer, and even the free troposphere as part of aerosol particles. The relationship between ground-level and high-altitude measurements was strongly influenced by meteorological conditions and the mixing state of the lower atmosphere, as discussed in three representative cases. Long-range transport of Na^{+}_{aer} and $CCHO_{aer}$ from remote marine sources is presumably relevant for high-altitude measurements, especially when the upper air masses were decoupled from the ground. However, in cases of a well-mixed lower atmosphere, the local marine source (here, the Kongsfjorden) was the dominant contributor for atmospheric Na^{+}_{aer} and $CCHO_{aer}$. Under very humid conditions particularly in the presence of liquid precipitating clouds, in-situ formation of $CCHO_{aer}$ was observed, possibly linked to microbial metabolism. To establish more generalizable patterns, we recommend further field studies using airborne platforms.

The significant correlation between combined xylose within $CCHO_{aer}$, and $oxalate_{aer}$ suggests underlying pathways for oxalic acid formation from combined xylose and other monosaccharide units within $CCHO_{aer}$; alternatively, a co-production of xylose-containing oligo- and polysaccharides alongside oxalate precursors.

Cloud condensation nuclei and ice-nucleating particles are key drivers in cloud formation, influencing radiative and precipitation properties and, consequently, climate processes. Considerable uncertainties remain regarding the origin and chemical composition of these particles, particularly in remote Arctic regions, which affects the accuracy of climate models. Since marine polysaccharides have been identified as relevant ice-nucleating molecules in the remote marine atmosphere (Hartmann et al., 2025), our findings have implications for cloud microphysics, especially given that these carbohydrates are transported to altitudes relevant for cloud formation. Furthermore, atmospheric processing, as observed here, may alter the ice-nucleating properties of these macromolecules, potentially creating new ice-nucleating particles in-situ or deactivating existing ones.

As the Arctic continues to change, expanding ice-free ocean areas will serve as emission sources for SSA particles, influencing cloud properties, and finally the radiative budget.

Consequently, our findings contribute to an improved understanding of the complex interplay of environmental processes resulting in Arctic amplification (Wendisch et al., 2017, 2023).

Author contributions

SZ wrote the manuscript with input from all co-authors. SZ, JS, CP, HS, BW, MW, and MvP collected field samples in Ny-Ålesund. HS and BW served as principal investigators for balloon operations during the field campaign. SZ conducted the laboratory carbohydrate analyses and data processing. MZ and AB carried out the FESOM2.1-REcoM3 simulations. KE assessed cloud conditions for the case studies using remote sensing data. All co-authors reviewed and commented on the manuscript.

Acknowledgments

We would like to express our gratitude to Kings Bay and the AWIPEV staff, with special thanks to the station leader Grégory Tran, for their invaluable support to make this field study possible. We furthermore thank the AWIPEV station's scientific staff in ensuring the availability of high-quality meteorological data. In this context, we like to give special thanks to Fieke Rader and Marion Maturilli. The cloud observations were taken within the project AWIPEV_0016.

We also thank the scientific team at the Zeppelin Observatory from NILU and NPI, with special appreciation to Wenche Aas, for their dedicated work in monitoring aerosol data.

Furthermore, we acknowledge the entire BELUGA team for their contributions during both the autumn 2021 and spring 2022 campaigns, with special thanks to Thomas Conrath. We also thank Michel Michalkow for preprocessing the CAMP and standard meteorological data collected at BELUGA as part of his Master's thesis. We are grateful to René Rabe for preparing the campaign equipment and to Leon Schmidt for conducting the chemical analysis of inorganic ions.

For the FESOM2.1-REcoM3 simulation for this research, the authors gratefully acknowledge the computing time granted by the Resource Allocation Board and provided on the supercomputer Lise and Emmy at NHR@ZIB and NHR@Göttingen as part of the NHR

infrastructure. The calculations for this research were conducted with computing resources under the project hbk00084.

This research has been supported by the Deutsche Forschungsgemeinschaft (DFG, German Research Foundation, project no. 268020496-TRR 172) within the Transregional Collaborative Research Center "ArctiC Amplification: Climate Relevant Atmospheric and SurfaCe Processes, and Feedback Mechanisms (AC)3" in subprojects A02, B04, C03 and E02. MW was supported by the DFG Priority Program SPP 1158 "Antarctic Research with comparative investigations in Arctic ice areas" (grant 522416631). We thank Johannes Röttenbacher for his constructive feedback on the manuscript.

Competing interests

All authors declare no financial or non-financial competing interests. Some authors are members of the editorial board of ACP.

Data availability

Chemical data from offline TSP filters are publicly available in PANGAEA for seawater (Zeppenfeld and Schmidt, 2025) and aerosol particles (Zeppenfeld et al., 2025). The microwave radiometer LWP and IWV data are available in PANGAEA (Ebell and Ritter, 2022). The Cloudnet classification and ice water content products (Ebell et al., 2025) can be downloaded via the ACTRIS Cloudnet data portal (https://cloudnet.fmi.fi).

References

Aas, W., Berglen, T. F., Eckhardt, S., Fiebig, M., Solberg, S., and Yttri, K. E.: Monitoring of long-range transported air pollutants in Norway. Annual Report 2021., NILU, 2022.

Aas, W., Eckhardt, S., Solberg, S., and Yttri, K. E.: Monitoring of long-range transported air pollutants in Norway. Annual Report 2022., NILU, 2023.

Akansu, E. F., Dahlke, S., Siebert, H., and Wendisch, M.: Evaluation of methods to determine the surface mixing layer height of the atmospheric boundary layer in the central Arctic during polar night and transition to polar day in cloudless and cloudy conditions, Atmospheric Chemistry and Physics, 23, 15473–15489, https://doi.org/10.5194/acp-23-15473-2023, 2023.

Aller, J. Y., Kuznetsova, M. R., Jahns, C. J., and Kemp, P. F.: The sea surface microlayer as a source of viral and bacterial enrichment in marine aerosols, Journal of Aerosol Science, 36, 801–812, https://doi.org/10.1016/j.jaerosci.2004.10.012, 2005.

Aller, J. Y., Radway, J. C., Kilthau, W. P., Bothe, D. W., Wilson, T. W., Vaillancourt, R. D., Quinn, P. K., Coffman, D. J., Murray, B. J., and Knopf, D. A.: Size-resolved characterization of the polysaccharidic and proteinaceous components of sea spray aerosol, Atmospheric Environment, 154, 331–347, https://doi.org/10.1016/j.atmosenv.2017.01.053, 2017.

Alpert, P. A., Kilthau, W. P., O'Brien, R. E., Moffet, R. C., Gilles, M. K., Wang, B., Laskin, A., Aller, J. Y., and Knopf, D. A.: Ice-nucleating agents in sea spray aerosol identified and quantified with a holistic multimodal freezing model, Science Advances, 8, eabq6842, https://doi.org/10.1126/sciadv.abq6842, 2022.

Aluwihare, L. I., Repeta, D. J., and Chen, R. F.: A major biopolymeric component to dissolved organic carbon in surface sea water, Nature, 387, 166–169, https://doi.org/10.1038/387166a0, 1997.

Amore, A., Giardi, F., Becagli, S., Caiazzo, L., Mazzola, M., Severi, M., and Traversi, R.: Source apportionment of sulphate in the High Arctic by a 10 yr-long record from Gruvebadet Observatory (Ny-Ålesund, Svalbard Islands), Atmospheric Environment, 270, 118890, https://doi.org/10.1016/j.atmosenv.2021.118890, 2022.

Angle, K., Grassian, V. H., and Ault, A. P.: The rapid acidification of sea spray aerosols, Physics today, 75, 58–59, https://doi.org/10.1063/PT.3.4926, 2022.

Angle, K. J., Crocker, D. R., Simpson, R. M. C., Mayer, K. J., Garofalo, L. A., Moore, A. N., Garcia, S. L. M., Or, V. W., Srinivasan, S., Farhan, M., Sauer, J. S., Lee, C., Pothier, M. A., Farmer, D. K., Martz, T. R., Bertram, T. H., Cappa, C. D., Prather, K. A., and Grassian, V. H.: Acidity across the interface from the ocean surface to sea spray aerosol, PNAS, 118, 1–6, https://doi.org/10.1073/pnas.2018397118, 2021.

Arnosti, C., Wietz, M., Brinkhoff, T., Hehemann, J.-H., Probandt, D., Zeugner, L., and Amann, R.: The Biogeochemistry of Marine Polysaccharides: Sources, Inventories, and Bacterial Drivers of the Carbohydrate Cycle, Ann Rev Mar Sci, 13, 81–108, https://doi.org/10.1146/annurev-marine-032020-012810, 2021.

Assmy, P., Cecilie Kvernvik, A., Hop, H., Hoppe, C. J. M., Chierici, M., David T., D., Duarte, P., Fransson, A., García, L. M., Patuła, W., Kwaśniewski, S., Maturilli, M., Pavlova, O., Tatarek, A., Wiktor, J. M., Wold, A., Wolf, K. K. E., and Bailey, A.: Seasonal plankton dynamics in Kongsfjorden during two years of contrasting environmental conditions, Progress in Oceanography, 213, 102996, https://doi.org/10.1016/j.pocean.2023.102996, 2023.

Avcı, B., Krüger, K., Fuchs, B. M., Teeling, H., and Amann, R. I.: Polysaccharide niche partitioning of distinct Polaribacter clades during North Sea spring algal blooms, ISME J, 14, 1369–1383, https://doi.org/10.1038/s41396-020-0601-y, 2020.

Barthelmeß, T., Cristi, A., Deppeler, S., Safi, K., Sellegri, K., Law, C. S., and Engel, A.: Pronounced Diel Cycling of Dissolved Carbohydrates and Amino Acids in the Surface Ocean and across Diverse Regimes, Environ. Sci. Technol., 59, 419–429, https://doi.org/10.1021/acs.est.4c00491, 2025.

Becker, S., Tebben, J., Coffinet, S., Wiltshire, K., Iversen, M. H., Harder, T., Hinrichs, K.-U., and Hehemann, J.-H.: Laminarin is a major molecule in the marine carbon cycle, PNAS, 117, 6599–6607, https://doi.org/10.1073/pnas.1917001117, 2020.

Bianco, A., Deguillaume, L., Chaumerliac, N., Vaïtilingom, M., Wang, M., Delort, A.-M., and Bridoux, M. C.: Effect of endogenous microbiota on the molecular composition of cloud water: a study by Fourier-transform ion cyclotron resonance mass spectrometry (FT-ICR MS), Sci Rep, 9, 1–12, https://doi.org/10.1038/s41598-019-44149-8, 2019.

Bischof, K., Convey, P., Duarte, P., Gattuso, J.-P., Granberg, M., Hop, H., Hoppe, C., Jiménez, C., Lisitsyn, L., Martinez, B., Roleda, M. Y., Thor, P., Wiktor, J. M., and Gabrielsen, G. W.: Kongsfjorden as Harbinger of the Future Arctic: Knowns, Unknowns and Research Priorities, in: The Ecosystem of Kongsfjorden, Svalbard, edited by: Hop, H. and Wiencke, C., Springer International Publishing, Cham, 537–562, https://doi.org/10.1007/978-3-319-46425-1_14, 2019.

Bivand, R., Pebesma, E., and Gomez-Rubio, V.: Applied spatial data analysis with R, Springer, 2013.

Bivand, R., Keitt, T., and Rowlingson, B.: rgdal: Bindings for the "Geospatial" Data Abstraction Library, R package version 1.5-32, 2022.

Borch, N. H. and Kirchman, D. L.: Concentration and composition of dissolved combined neutral sugars (polysaccharides) in seawater determined by HPLC-PAD, Marine Chemistry, 57, 85–95, https://doi.org/10.1016/S0304-4203(97)00002-9, 1997.

Brownrigg, M. R.: Package 'mapdata, R package version 2.3.1, 2013.

Brownrigg, M. R.: maps: Draw Geographical Maps, R package version 3.4.2, 2023.

Browse, J., Carslaw, K. S., Mann, G. W., Birch, C. E., Arnold, S. R., and Leck, C.: The complex response of Arctic aerosol to sea-ice retreat, Atmospheric Chemistry and Physics, 14, 7543–7557, https://doi.org/10.5194/acp-14-7543-2014, 2014.

Burns, W. G., Marchetti, A., and Ziervogel, K.: Enhanced formation of transparent exopolymer particles (TEP) under turbulence during phytoplankton growth, J Plankton Res, 41, 349–361, https://doi.org/10.1093/plankt/fbz018, 2019.

Burrows, S. M., Ogunro, O., Frossard, A., Russell, L. M., Rasch, P. J., and Elliott, S.: A Physically Based Framework for Modelling the Organic Fractionation of Sea Spray Aerosol from Bubble Film Langmuir Equilibria, Atmospheric Chemistry and Physics, 14(24):13601–13629, https://doi.org/10.5194/acp-14-13601-2014, 2014.

Cai, Q., Wang, J., Beletsky, D., Overland, J., Ikeda, M., and Wan, L.: Accelerated decline of summer Arctic sea ice during 1850–2017 and the amplified Arctic warming during the recent decades, Environ. Res. Lett., 16, 034015, https://doi.org/10.1088/1748-9326/abdb5f, 2021.

Carlton, A. G., Wiedinmyer, C., and Kroll, J. H.: A review of Secondary Organic Aerosol (SOA) formation from isoprene, Atmospheric Chemistry and Physics, 9, 4987–5005, https://doi.org/10.5194/acp-9-4987-2009, 2009.

Carslaw, D. C. and Ropkins, K.: openair --- An R package for air quality data analysis, Environmental Modelling & Software, 27–28, 52–61, 2012.

Chang, L., Song, S., Feng, G., Zhang, Y., and Gao, G.: Assessment of the Uncertainties in Arctic Low-Level Temperature Inversion Characteristics in Radio Occultation Observations, IEEE Transactions on Geoscience and Remote Sensing, 55, 1793–1803, https://doi.org/10.1109/TGRS.2016.2633461, 2017.

Chi, J. W., Li, W. J., Zhang, D. Z., Zhang, J. C., Lin, Y. T., Shen, X. J., Sun, J. Y., Chen, J. M., Zhang, X. Y., Zhang, Y. M., and Wang, W. X.: Sea salt aerosols as a reactive surface for inorganic and organic acidic gases in the Arctic troposphere, Atmospheric Chemistry and Physics, 15, 11341–11353, https://doi.org/10.5194/acp-15-11341-2015, 2015.

Compiano, A.-M., Romano, J.-C., Garabetian, F., Laborde, P., and de la Giraudièrea, I.: Monosaccharide composition of particulate hydrolysable sugar fraction in surface microlayers from brackish and marine waters, Marine Chemistry, 42, 237–251, https://doi.org/10.1016/0304-4203(93)90015-G, 1993.

Crahan, K. K., Hegg, D., Covert, D. S., and Jonsson, H.: An exploration of aqueous oxalic acid production in the coastal marine atmosphere, Atmospheric Environment, 38, 3757–3764, https://doi.org/10.1016/j.atmosenv.2004.04.009, 2004.

Creamean, J. M., de Boer, G., Telg, H., Mei, F., Dexheimer, D., Shupe, M. D., Solomon, A., and McComiskey, A.: Assessing the vertical structure of Arctic aerosols using balloon-borne measurements, Atmospheric Chemistry and Physics, 21, 1737–1757, https://doi.org/10.5194/acp-21-1737-2021, 2021.

Croft, B., Lohmann, U., Martin, R. V., Stier, P., Wurzler, S., Feichter, J., Posselt, R., and Ferrachat, S.: Aerosol size-dependent below-cloud scavenging by rain and snow in the ECHAM5-HAM, Atmospheric Chemistry and Physics, 9, 4653–4675, https://doi.org/10.5194/acp-9-4653-2009, 2009.

Cunliffe, M. and Wurl, O.: Guide to best practices to study the ocean's surface., Marine Biological Association of the United Kingdom for SCOR, 2014.

Dahms, A. S.: 3-Deoxy-D-pentulosonic acid aldolase and its role in a new pathway of D-xylose degradation, Biochemical and Biophysical Research Communications, 60, 1433–1439, https://doi.org/10.1016/0006-291X(74)90358-1, 1974.

Dekhtyareva, A., Holmén, K., Maturilli, M., Hermansen, O., and Graversen, R.: Effect of seasonal mesoscale and microscale meteorological conditions in Ny-Ålesund on results of monitoring of long-range transported pollution, Polar Research, 2018.

DeMott, P. J., Hill, T. C. J., McCluskey, C. S., Prather, K. A., Collins, D. B., Sullivan, R. C., Ruppel, M. J., Mason, R. H., Irish, V. E., Lee, T., Hwang, C. Y., Rhee, T. S., Snider, J. R., McMeeking, G. R., Dhaniyala, S., Lewis, E. R., Wentzell, J. J. B., Abbatt, J., Lee, C., Sultana, C. M., Ault, A. P., Axson, J. L., Martinez, M. D., Venero, I., Santos-Figueroa, G., Stokes, M. D., Deane, G. B., Mayol-Bracero, O. L., Grassian, V. H., Bertram, T. H., Bertram, A. K., Moffett, B. F., and Franc, G. D.: Sea spray aerosol as a unique source of ice nucleating particles, PNAS, 113, 5797–5803, https://doi.org/10.1073/pnas.1514034112, 2016.

Dusek, U., Frank, G. P., Hildebrandt, L., Curtius, J., Schneider, J., Walter, S., Chand, D., Drewnick, F., Hings, S., Jung, D., Borrmann, S., and Andreae, M. O.: Size Matters More Than Chemistry for Cloud-Nucleating Ability of Aerosol Particles, Science, 312, 1375–1378, https://doi.org/10.1126/science.1125261, 2006.

Ebell, K. and Ritter, C.: HATPRO microwave radiometer measurements at AWIPEV, Ny-Ålesund (2019-2021), PANGAEA, https://doi.org/10.1594/PANGAEA.943004, 2022.

Ebell, K., Maturilli, M., Ritter, C., and O'Connor, E.: Custom collection of classification, and ice water content data from Ny-Ålesund between 27 Sep and 12 Nov 2021, ACTRIS Cloud remote sensing data centre unit (CLU), https://doi.org/10.60656/5598100185854c01, 2025.

Egerer, U., Ehrlich, A., Gottschalk, M., Griesche, H., Neggers, R. A. J., Siebert, H., and Wendisch, M.: Case study of a humidity layer above Arctic stratocumulus and potential turbulent coupling with the cloud top, Atmospheric Chemistry and Physics, 21, 6347–6364, https://doi.org/10.5194/acp-21-6347-2021, 2021.

Egerer, U., Siebert, H., Hellmuth, O., and Sørensen, L. L.: The role of a low-level jet for stirring the stable atmospheric surface layer in the Arctic, Atmospheric Chemistry and Physics, 23, 15365–15373, https://doi.org/10.5194/acp-23-15365-2023, 2023.

Engel, A.: Distribution of transparent exopolymer particles (TEP) in the northeast Atlantic Ocean and their potential significance for aggregation processes, Deep Sea Research Part I: Oceanographic Research Papers, 51, 83–92, https://doi.org/10.1016/j.dsr.2003.09.001, 2004.

Engel, A. and Galgani, L.: The organic sea-surface microlayer in the upwelling region off the coast of Peru and potential implications for air–sea exchange processes, Biogeosciences (BG), 13, 989–1007, https://doi.org/10.5194/bg-13-989-2016, 2016.

Engel, A. and Händel, N.: A novel protocol for determining the concentration and composition of sugars in particulate and in high molecular weight dissolved organic matter (HMW-DOM) in seawater, Marine Chemistry, 127, 180–191, https://doi.org/10.1016/j.marchem.2011.09.004, 2011.

Engel, A., Thoms, S., Riebesell, U., Rochelle-Newall, E., and Zondervan, I.: Polysaccharide aggregation as a potential sink of marine dissolved organic carbon, Nature, 428, 929–932, https://doi.org/10.1038/nature02453, 2004.

Engel, A., Harlay, J., Piontek, J., and Chou, L.: Contribution of combined carbohydrates to dissolved and particulate organic carbon after the spring bloom in the northern Bay of Biscay (North-Eastern Atlantic Ocean), Continental Shelf Research, 45, 42–53, https://doi.org/10.1016/j.csr.2012.05.016, 2012.

Ervens, B. and Amato, P.: The global impact of bacterial processes on carbon mass, Atmospheric Chemistry & Physics, 20, 1777–1794, https://doi.org/10.5194/acp-20-1777-2020, 2020.

Esau, I. and Repina, I.: Wind Climate in Kongsfjorden, Svalbard, and Attribution of Leading Wind Driving Mechanisms through Turbulence-Resolving Simulations, Advances in Meteorology, 2012, 568454, https://doi.org/10.1155/2012/568454, 2012.

Fabiano, M., Povero, P., and Danovaro, R.: Distribution and composition of particulate organic matter in the Ross Sea (Antarctica), Polar Biol, 13, 525–533, https://doi.org/10.1007/BF00236394, 1993.

Facchini, M. C., Rinaldi, M., Decesari, S., Carbone, C., Finessi, E., Mircea, M., Fuzzi, S., Ceburnis, D., Flanagan, R., Nilsson, E. D., Leeuw, G. de, Martino, M., Woeltjen, J., and O'Dowd, C. D.: Primary submicron marine aerosol dominated by insoluble organic colloids and aggregates, Geophysical Research Letters, 35, 1–5, https://doi.org/10.1029/2008GL034210, 2008.

Farmer, D. K., Cappa, C. D., and Kreidenweis, S. M.: Atmospheric Processes and Their Controlling Influence on Cloud Condensation Nuclei Activity, Chem. Rev., 115, 4199–4217, https://doi.org/10.1021/cr5006292, 2015.

Farmer, D. K., Boedicker, E. K., and DeBolt, H. M.: Dry Deposition of Atmospheric Aerosols: Approaches, Observations, and Mechanisms, Annual Review of Physical Chemistry, 72, 375–397, https://doi.org/10.1146/annurev-physchem-090519-034936, 2021.

Feltracco, M., Barbaro, E., Hoppe, C. J. M., Wolf, K. K. E., Spolaor, A., Layton, R., Keuschnig, C., Barbante, C., Gambaro, A., and Larose, C.: Airborne bacteria and particulate chemistry capture Phytoplankton bloom dynamics in an Arctic fjord, Atmospheric Environment, 256, 118458, https://doi.org/10.1016/j.atmosenv.2021.118458, 2021.

Fomba, K. W., Müller, K., van Pinxteren, D., Poulain, L., van Pinxteren, M., and Herrmann, H.: Long-term chemical characterization of tropical and marine aerosols at the Cape Verde Atmospheric Observatory (CVAO) from 2007 to 2011, Atmospheric Chemistry and Physics, 14, 8883–8904, https://doi.org/10.5194/acp-14-8883-2014, 2014.

Francis, J. A. and Wu, B.: Why has no new record-minimum Arctic sea-ice extent occurred since September 2012?, Environ. Res. Lett., 15, 114034, https://doi.org/10.1088/1748-9326/abc047, 2020.

Freud, E., Krejci, R., Tunved, P., Leaitch, R., Nguyen, Q. T., Massling, A., Skov, H., and Barrie, L.: Pan-Arctic aerosol number size distributions: seasonality and transport patterns, Atmospheric Chemistry and Physics, 17, 8101–8128, https://doi.org/10.5194/acp-17-8101-2017, 2017.

Furukawa, T. and Takahashi, Y.: Oxalate metal complexes in aerosol particles: implications for the hygroscopicity of oxalate-containing particles, Atmos. Chem. Phys., 11, 4289–4301, https://doi.org/10.5194/acp-11-4289-2011, 2011.

Gantt, B., Meskhidze, N., Facchini, M. C., Rinaldi, M., Ceburnis, D., and O'Dowd, C. D.: Wind speed dependent size-resolved parameterization for the organic mass fraction of sea spray aerosol, Atmospheric Chemistry and Physics, 11, 8777–8790, https://doi.org/10.5194/acp-11-8777-2011, 2011.

Gao, Q., Leck, C., Rauschenberg, C., and Matrai, P. A.: On the chemical dynamics of extracellular polysaccharides in the high Arctic surface microlayer, Ocean Science, 8, 401–418, https://doi.org/10.5194/os-8-401-2012, 2012.

Gierens, R., Kneifel, S., Shupe, M. D., Ebell, K., Maturilli, M., and Löhnert, U.: Low-level mixed-phase clouds in a complex Arctic environment, Atmospheric Chemistry and Physics, 20, 3459–3481, https://doi.org/10.5194/acp-20-3459-2020, 2020.

Goldberg, S. J., Carlson, C. A., Brzezinski, M., Nelson, N. B., and Siegel, D. A.: Systematic removal of neutral sugars within dissolved organic matter across ocean basins, Geophysical Research Letters, 38, 1–7, https://doi.org/10.1029/2011GL048620, 2011.

Grawe, S., Jentzsch, C., Schaefer, J., Wex, H., Mertes, S., and Stratmann, F.: Next-generation ice-nucleating particle sampling on board aircraft: characterization of the High-volume flow aERosol particle filter sAmpler (HERA), Atmospheric Measurement Techniques, 16, 4551–4570, https://doi.org/10.5194/amt-16-4551-2023, 2023.

Grolemund, G. and Wickham, H.: Dates and Times Made Easy with lubridate, Journal of Statistical Software, 40, 1–25, 2011.

Grosse, J., Nöthig, E.-M., Torres-Valdés, S., and Engel, A.: Summertime Amino Acid and Carbohydrate Patterns in Particulate and Dissolved Organic Carbon Across Fram Strait, Front. Mar. Sci., 8, https://doi.org/10.3389/fmars.2021.684675, 2021.

Guo, T., Li, K., Zhu, Y., Gao, H., and Yao, X.: Concentration and size distribution of particulate oxalate in marine and coastal atmospheres – Implication for the increased importance of oxalate in nanometer atmospheric particles, Atmospheric Environment, 142, 19–31, https://doi.org/10.1016/j.atmosenv.2016.07.026, 2016.

Gürses, Ö., Oziel, L., Karakuş, O., Sidorenko, D., Völker, C., Ye, Y., Zeising, M., Butzin, M., and Hauck, J.: Ocean biogeochemistry in the coupled ocean–sea ice–biogeochemistry model FESOM2.1–REcoM3, Geoscientific Model Development, 16, 4883–4936, https://doi.org/10.5194/gmd-16-4883-2023, 2023.

Haddrell, A. E. and Thomas, R. J.: Aerobiology: Experimental Considerations, Observations, and Future Tools, Appl. Environ. Microbiol., 83, 1–15, https://doi.org/10.1128/AEM.00809-17, 2017.

Hansell, D. A.: Recalcitrant Dissolved Organic Carbon Fractions, Annual Review of Marine Science, 5, 421–445, https://doi.org/10.1146/annurev-marine-120710-100757, 2013.

Hara, K., Yamagata, S., Yamanouchi, T., Sato, K., Herber, A., Iwasaka, Y., Nagatani, M., and Nakata, H.: Mixing states of individual aerosol particles in spring Arctic troposphere during ASTAR 2000 campaign, Journal of Geophysical Research: Atmospheres, 108, 1–12, https://doi.org/10.1029/2002JD002513, 2003.

Hartmann, S., Schrödner, R., Hassett, B. T., Hartmann, M., van Pinxteren, M., Fomba, K. W., Stratmann, F., Herrmann, H., Pöhlker, M., and Zeppenfeld, S.: Polysaccharides–Important Constituents of Ice-Nucleating Particles of Marine Origin, Environ. Sci. Technol., 59, 5098–5108, https://doi.org/10.1021/acs.est.4c08014, 2025.

Hasenecz, E., Jayarathne, T., Pendergraft, M. A., Santander, M. V., Mayer, K. J., Sauer, J., Lee, C., Gibson, W. S., Kruse, S. M., Malfatti, F., Prather, K. A., and Stone, E. A.: Marine bacteria affect saccharide enrichment in sea spray aerosol during a phytoplankton bloom, ACS Earth Space Chem., 4, 1638–1649, https://doi.org/10.1021/acsearthspacechem.0c00167, 2020.

Hasenecz, E. S., Kaluarachchi, C. P., Lee, H. D., Tivanski, A. V., and Stone, E. A.: Saccharide Transfer to Sea Spray Aerosol Enhanced by Surface Activity, Calcium, and Protein Interactions, ACS Earth Space Chem., 3, 2539–2548, https://doi.org/10.1021/acsearthspacechem.9b00197, 2019.

Herrmann, H., Tilgner, A., Barzaghi, P., Majdik, Z., Gligorovski, S., Poulain, L., and Monod, A.: Towards a more detailed description of tropospheric aqueous phase organic chemistry: CAPRAM 3.0, Atmospheric Environment, 39, 4351–4363, https://doi.org/10.1016/j.atmosenv.2005.02.016, 2005.

Heutte, B., Bergner, N., Angot, H., Pernov, J. B., Dada, L., Mirrielees, J. A., Beck, I., Baccarini, A., Boyer, M., Creamean, J. M., Daellenbach, K. R., El Haddad, I., Frey, M. M., Henning, S., Laurila, T., Moschos, V., Petäjä, T., Pratt, K. A., Quéléver, L. L. J., Shupe, M. D., Zieger, P., Jokinen, T., and Schmale, J.: Observations of high-time-resolution and size-resolved aerosol chemical composition and microphysics in the central Arctic: implications for climate-relevant particle properties, Atmospheric Chemistry and Physics, 25, 2207–2241, https://doi.org/10.5194/acp-25-2207-2025, 2025.

Hijmans, R. J.: raster: Geographic Data Analysis and Modeling, R package version 3.6-26, 2023.

Hill, T. C. J., Malfatti, F., McCluskey, C. S., Schill, G. P., Santander, M. V., Moore, K. A., Rauker, A. M., Perkins, R. J., Celussi, M., Levin, E. J. T., Suski, K. J., Cornwell, G. C., Lee, C., Negro, P. D., Kreidenweis, S. M., Prather, K. A., and DeMott, P. J.: Resolving the controls over the production and emission of ice-nucleating particles in sea spray, Environ. Sci.: Atmos., https://doi.org/10.1039/D2EA00154C, 2023.

Hoffman, E. J. and Duce, R. A.: Factors influencing the organic carbon content of marine aerosols: A laboratory study, Journal of Geophysical Research (1896-1977), 81, 3667–3670, https://doi.org/10.1029/JC081i021p03667, 1976.

Hogan, R. J., Mittermaier, M. P., and Illingworth, A. J.: The Retrieval of Ice Water Content from Radar Reflectivity Factor and Temperature and Its Use in Evaluating a Mesoscale Model, Journal of Applied Meteorology and Climatology, 45, 301–317, https://doi.org/10.1175/JAM2340.1, 2006.

Hoppel, W. A., Frick, G. M., and Fitzgerald, J. W.: Surface source function for sea-salt aerosol and aerosol dry deposition to the ocean surface, Journal of Geophysical Research: Atmospheres, 107, AAC 7-1-AAC 7-17, https://doi.org/10.1029/2001JD002014, 2002.

Illingworth, A. J., Hogan, R. J., O'Connor, E. J., Bouniol, D., Brooks, M. E., Delanoé, J., Donovan, D. P., Eastment, J. D., Gaussiat, N., Goddard, J. W. F., Haeffelin, M., Baltink, H. K., Krasnov, O. A., Pelon, J., Piriou, J.-M., Protat, A., Russchenberg, H. W. J., Seifert, A., Tompkins, A. M., Zadelhoff, G.-J. van, Vinit, F., Willén, U., Wilson, D. R., and Wrench, C. L.: Cloudnet: Continuous

Evaluation of Cloud Profiles in Seven Operational Models Using Ground-Based Observations, Bulletin of the American Meteorological Society, 88, 883–898, https://doi.org/10.1175/BAMS-88-6-883, 2007.

Ittekkot, V., Brockmann, U., Michaelis, W., and Degens, E. T.: Dissolved free and combined carbohydrates during a phytoplankton bloom in the northern North Sea, Marine Ecology Progress Series, 4, 299–305, 1981.

Jayarathne, T., Sultana, C. M., Lee, C., Malfatti, F., Cox, J. L., Pendergraft, M. A., Moore, K. A., Azam, F., Tivanski, A. V., Cappa, C. D., Bertram, T. H., Grassian, V. H., Prather, K. A., and Stone, E. A.: Enrichment of Saccharides and Divalent Cations in Sea Spray Aerosol During Two Phytoplankton Blooms, Environ Sci Technol, 50, 11511–11520, https://doi.org/10.1021/acs.est.6b02988, 2016.

Jensen, L. Z., Glasius, M., Gryning, S.-E., Massling, A., Finster, K., and Šantl-Temkiv, T.: Seasonal Variation of the Atmospheric Bacterial Community in the Greenlandic High Arctic Is Influenced by Weather Events and Local and Distant Sources, Front. Microbiol., 13, https://doi.org/10.3389/fmicb.2022.909980, 2022.

Kang, H., Jung, C. H., Lee, B. Y., Krejci, R., Heslin-Rees, D., Aas, W., and Yoon, Y. J.: Aerosol hygroscopicity influenced by seasonal chemical composition variations in the Arctic region, Journal of Aerosol Science, 106551, https://doi.org/10.1016/j.jaerosci.2025.106551, 2025.

Kanji, Z. A., Ladino, L. A., Wex, H., Boose, Y., Burkert-Kohn, M., Cziczo, D. J., and Krämer, M.: Overview of Ice Nucleating Particles, Meteorological Monographs, 58, 1.1-1.33, https://doi.org/10.1175/AMSMONOGRAPHS-D-16-0006.1, 2017.

Karl, M., Leck, C., Rad, F. M., Bäcklund, A., Lopez-Aparicio, S., and Heintzenberg, J.: New insights in sources of the sub-micrometre aerosol at Mt. Zeppelin observatory (Spitsbergen) in the year 2015, Tellus B: Chemical and Physical Meteorology, 71, 1613143, https://doi.org/10.1080/16000889.2019.1613143, 2019.

Kawamura, K. and Bikkina, S.: A review of dicarboxylic acids and related compounds in atmospheric aerosols: Molecular distributions, sources and transformation, Atmospheric Research, 170, 140–160, https://doi.org/10.1016/j.atmosres.2015.11.018, 2016.

Kawamura, K., Kasukabe, H., and Barrie, L. A.: Source and reaction pathways of dicarboxylic acids, ketoacids and dicarbonyls in arctic aerosols: One year of observations, Atmospheric Environment, 30, 1709–1722, https://doi.org/10.1016/1352-2310(95)00395-9, 1996a.

Kawamura, K., Sempéré, R., Imai, Y., Fujii, Y., and Hayashi, M.: Water soluble dicarboxylic acids and related compounds in Antarctic aerosols, Journal of Geophysical Research: Atmospheres, 101, 18721–18728, https://doi.org/10.1029/96JD01541, 1996b.

Keene, W. C., Pszenny, A. A. P., Galloway, J. N., and Hawley, M. E.: Sea-salt corrections and interpretation of constituent ratios in marine precipitation, Journal of Geophysical Research, 91, 6647–6658, https://doi.org/10.1029/JD091iD06p06647, 1986.

Keene, W. C., Long, M. S., Reid, J. S., Frossard, A. A., Kieber, D. J., Maben, J. R., Russell, L. M., Kinsey, J. D., Quinn, P. K., and Bates, T. S.: Factors That Modulate Properties of Primary Marine Aerosol Generated From Ambient Seawater on Ships at Sea, Journal of Geophysical Research: Atmospheres, 122, 11,961-11,990, https://doi.org/10.1002/2017JD026872, 2017.

Kerminen, V.-M., Teinilä, K., Hillamo, R., and Mäkelä, T.: Size-segregated chemistry of particulate dicarboxylic acids in the Arctic atmosphere, Atmospheric Environment, 33, 2089–2100, https://doi.org/10.1016/S1352-2310(98)00350-1, 1999.

Khadem, H. E.: Carbohydrate Chemistry: Monosaccharides and Their Oligomers, Elsevier, 267 pp., 2012.

Kharbush, J. J., Close, H. G., Van Mooy, B. A. S., Arnosti, C., Smittenberg, R. H., Le Moigne, F. A. C., Mollenhauer, G., Scholz-Böttcher, B., Obreht, I., Koch, B. P., Becker, K., Iversen, M. H., and Mohr, W.: Particulate Organic Carbon Deconstructed: Molecular and Chemical Composition of Particulate Organic Carbon in the Ocean, Frontiers in Marine Science, 7, Art.Nr. 518, https://doi.org/10.3389/fmars.2020.00518, 2020.

Kirchman, D. L., Meon, B., Ducklow, H. W., Carlson, C. A., Hansell, D. A., and Steward, G. F.: Glucose fluxes and concentrations of dissolved combined neutral sugars (polysaccharides) in the Ross Sea and Polar Front Zone, Antarctica, Deep Sea Research Part II: Topical Studies in Oceanography, 48, 4179–4197, https://doi.org/10.1016/S0967-0645(01)00085-6, 2001.

Klein, A. M., Bohannan, B. J. M., Jaffe, D. A., Levin, D. A., and Green, J. L.: Molecular Evidence for Metabolically Active Bacteria in the Atmosphere, Front. Microbiol., 7, 772, https://doi.org/10.3389/fmicb.2016.00772, 2016.

Köllner, F., Schneider, J., Willis, M. D., Klimach, T., Helleis, F., Bozem, H., Kunkel, D., Hoor, P., Burkart, J., Leaitch, W. R., Aliabadi, A. A., Abbatt, J. P. D., Herber, A. B., and Borrmann, S.: Particulate trimethylamine in the summertime Canadian high Arctic lower troposphere, Atmospheric Chemistry and Physics, 17, 13747–13766, https://doi.org/10.5194/acp-17-13747-2017, 2017.

Leck, C., Gao, Q., Mashayekhy Rad, F., and Nilsson, U.: Size-resolved atmospheric particulate polysaccharides in the high summer Arctic, Atmospheric Chemistry and Physics, 13, 12573–12588, https://doi.org/10.5194/acp-13-12573-2013, 2013.

Leon-Marcos, A., Zeising, M., van Pinxteren, M., Zeppenfeld, S., Bracher, A., Barbaro, E., Engel, A., Feltracco, M., Tegen, I., and Heinold, B.: Modelling emission and transport of key components of primary marine organic aerosol using the global aerosol–climate model ECHAM6.3–HAM2.3, Geoscientific Model Development, 18, 4183–4213, https://doi.org/10.5194/gmd-18-4183-2025, 2025.

Li, J., Han, Z., Fu, P., Yao, X., and Liang, M.: Seasonal characteristics of emission, distribution, and radiative effect of marine organic aerosols over the western Pacific Ocean: an investigation with a coupled regional climate aerosol model, Atmospheric Chemistry and Physics, 24, 3129–3161, https://doi.org/10.5194/acp-24-3129-2024, 2024.

Lohmann, U. and Feichter, J.: Global indirect aerosol effects: a review, Atmospheric Chemistry and Physics, 5, 715–737, https://doi.org/10.5194/acp-5-715-2005, 2005.

Madry, W. L., Toon, O. B., and O'Dowd, C. D.: Modeled optical thickness of sea-salt aerosol, Journal of Geophysical Research: Atmospheres, 116, https://doi.org/10.1029/2010JD014691, 2011.

Malfatti, F., Lee, C., Tinta, T., Pendergraft, M. A., Celussi, M., Zhou, Y., Sultana, C. M., Rotter, A., Axson, J. L., Collins, D. B., Santander, M. V., Anides Morales, A. L., Aluwihare, L. I., Riemer, N., Grassian, V. H., Azam, F., and Prather, K. A.: Detection of Active Microbial Enzymes in Nascent Sea Spray Aerosol: Implications for Atmospheric Chemistry and Climate, Environ. Sci. Technol. Lett., 6, 171–177, https://doi.org/10.1021/acs.estlett.8b00699, 2019.

Manders, A. M. M., Schaap, M., Querol, X., Albert, M. F. M. A., Vercauteren, J., Kuhlbusch, T. A. J., and Hoogerbrugge, R.: Sea salt concentrations across the European continent, Atmospheric Environment, 44, 2434–2442, https://doi.org/10.1016/j.atmosenv.2010.03.028, 2010.

Matulová, M., Husárová, S., Capek, P., Sancelme, M., and Delort, A.-M.: Biotransformation of Various Saccharides and Production of Exopolymeric Substances by Cloud-Borne Bacillus sp. 3B6, Environ. Sci. Technol., 48, 14238–14247, https://doi.org/10.1021/es501350s, 2014.

Maturilli, M.: Continuous meteorological observations at station Ny-Ålesund (2011-08 et seq), Alfred Wegener Institute - Research Unit Potsdam, https://doi.org/10.1594/PANGAEA.914979, 2020.

Maturilli, M., Herber, A., and König-Langlo, G.: Climatology and time series of surface meteorology in Ny-Ålesund, Svalbard, Earth System Science Data, 5, 155–163, https://doi.org/10.5194/essd-5-155-2013, 2013.

Maturilli, M., Herber, A., and König-Langlo, G.: Surface radiation climatology for Ny-Ålesund, Svalbard (78.9° N), basic observations for trend detection, Theor Appl Climatol, 120, 331–339, https://doi.org/10.1007/s00704-014-1173-4, 2015.

Mayot, N., Matrai, P., Ellingsen, I. H., Steele, M., Johnson, K., Riser, S. C., and Swift, D.: Assessing Phytoplankton Activities in the Seasonal Ice Zone of the Greenland Sea Over an Annual Cycle, Journal of Geophysical Research: Oceans, 123, 8004–8025, https://doi.org/10.1029/2018JC014271, 2018.

McNeill, V. F.: Aqueous Organic Chemistry in the Atmosphere: Sources and Chemical Processing of Organic Aerosols, Environ. Sci. Technol., 49, 1237–1244, https://doi.org/10.1021/es5043707, 2015.

Mirrielees, J. A., Kirpes, R. M., Costa, E. J., Porter, G. C. E., Murray, B. J., Lata, N. N., Boschi, V., China, S., Grannas, A. M., Ault, A. P., Matrai, P. A., and Pratt, K. A.: Marine aerosol generation experiments in the High Arctic during summertime, Elementa: Science of the Anthropocene, 12, 00134, https://doi.org/10.1525/elementa.2023.00134, 2024.

Müller, K., Lehmann, S., Pinxteren, D. van, Gnauk, T., Niedermeier, N., Wiedensohler, A., and Herrmann, H.: Particle characterization at the Cape Verde atmospheric observatory during the 2007 RHaMBLe intensive, Atmospheric Chemistry and Physics, 10, 2709–2721, https://doi.org/10.5194/acp-10-2709-2010, 2010.

Neuwirth, E.: RColorBrewer: ColorBrewer Palettes, R package version 1.1-3, 2022.

Nomokonova, T., Ebell, K., Löhnert, U., Maturilli, M., Ritter, C., and O'Connor, E.: Statistics on clouds and their relation to thermodynamic conditions at Ny-Ålesund using ground-based sensor synergy, Atmospheric Chemistry and Physics, 19, 4105–4126, https://doi.org/10.5194/acp-19-4105-2019, 2019.

O'Dowd, C. D. and de Leeuw, G.: Marine aerosol production: a review of the current knowledge, Philos Trans A Math Phys Eng Sci, 365, 1753–1774, https://doi.org/10.1098/rsta.2007.2043, 2007.

O'Dowd, C. D., Smith, M. H., Consterdine, I. E., and Lowe, J. A.: Marine aerosol, sea-salt, and the marine sulphur cycle: a short review, Atmospheric Environment, 31, 73–80, https://doi.org/10.1016/S1352-2310(96)00106-9, 1997.

Ooki, A., Uematsu, M., Miura, K., and Nakae, S.: Sources of sodium in atmospheric fine particles, Atmospheric Environment, 36, 4367–4374, https://doi.org/10.1016/S1352-2310(02)00341-2, 2002.

Orellana, M. V. and Leck, C.: Chapter 9 - Marine Microgels, in: Biogeochemistry of Marine Dissolved Organic Matter (Second Edition), edited by: Hansell, D. A. and Carlson, C. A., Academic Press, Boston, 451–480, https://doi.org/10.1016/B978-0-12-405940-5.00009-1, 2015.

Orellana, M. V., Matrai, P. A., Leck, C., Rauschenberg, C. D., Lee, A. M., and Coz, E.: Marine microgels as a source of cloud condensation nuclei in the high Arctic, PNAS, 108, 13612–13617, https://doi.org/10.1073/pnas.1102457108, 2011.

Oziel, L., Schourup-Kristensen, V., Wekerle, C., and Hauck, J.: The Pan-Arctic Continental Slope as an Intensifying Conveyer Belt for Nutrients in the Central Arctic Ocean (1985–2015), Global Biogeochemical Cycles, 36, e2021GB007268, https://doi.org/10.1029/2021GB007268, 2022.

Panagiotopoulos, C. and Sempéré, R.: Analytical methods for the determination of sugars in marine samples: A historical perspective and future directions, Limnology and Oceanography: Methods, 3, 419–454, https://doi.org/10.4319/lom.2005.3.419, 2005.

Penner, J. E., Andreae, M. O., Annegarn, H., Barrie, L., Feichter, J., Hegg, D., Jayaraman, A., Leaitch, R., Murphy, D., Nganga, J., and Pitari, G.: Aerosols, their Direct and Indirect Effects, Climate Change 2001: The Scientific Basis. Contribution of Working Group I to the Third Assessment Report of the Intergovernmental Panel on Climate Change, 289–348, 2001.

Pierce, D.: ncdf4: Interface to Unidata netCDF (Version 4 or Earlier) Format Data, R package version 1.22, 2023.

Pilinis, C., Pandis, S. N., and Seinfeld, J. H.: Sensitivity of direct climate forcing by atmospheric aerosols to aerosol size and composition, Journal of Geophysical Research, 100, 18,739-18,754, https://doi.org/10.1029/95JD02119, 1995.

Pilz, C., Düsing, S., Wehner, B., Müller, T., Siebert, H., Voigtländer, J., and Lonardi, M.: CAMP: an instrumented platform for balloon-borne aerosol particle studies in the lower atmosphere, Atmospheric Measurement Techniques, 15, 6889–6905, https://doi.org/10.5194/amt-15-6889-2022, 2022.

Pilz, C., Lonardi, M., Egerer, U., Siebert, H., Ehrlich, A., Heymsfield, A. J., Schmitt, C. G., Shupe, M. D., Wehner, B., and Wendisch, M.: Profile observations of the Arctic atmospheric boundary layer with the BELUGA tethered balloon during MOSAiC, Sci Data, 10, 534, https://doi.org/10.1038/s41597-023-02423-5, 2023.

Pilz, C., Cassano, J. J., de Boer, G., Kirbus, B., Lonardi, M., Pöhlker, M., Shupe, M. D., Siebert, H., Wendisch, M., and Wehner, B.: Tethered balloon measurements reveal enhanced aerosol occurrence aloft interacting with Arctic low-level clouds, Elementa: Science of the Anthropocene, 12, 00120, https://doi.org/10.1525/elementa.2023.00120, 2024.

van Pinxteren, M., Müller, C., Iinuma, Y., Stolle, C., and Herrmann, H.: Chemical Characterization of Dissolved Organic Compounds from Coastal Sea Surface Microlayers (Baltic Sea, Germany), Environmental Science & Technology, 46, 10455–10462, https://doi.org/10.1021/es204492b, 2012.

van Pinxteren, M., Barthel, S., Fomba, K. W., Müller, K., Von Tümpling, W., and Herrmann, H.: The influence of environmental drivers on the enrichment of organic carbon in the sea surface microlayer and in submicron aerosol particles – measurements from the Atlantic Ocean, Elem Sci Anth, 5, 1–21, https://doi.org/10.1525/elementa.225, 2017.

van Pinxteren, M., Robinson, T.-B., Zeppenfeld, S., Gong, X., Bahlmann, E., Fomba, K. W., Triesch, N., Stratmann, F., Wurl, O., Engel, A., Wex, H., and Herrmann, H.: High number concentrations of transparent exopolymer particles in ambient aerosol particles and cloud water – a case study at the tropical Atlantic Ocean, Atmospheric Chemistry and Physics, 22, 5725–5742, https://doi.org/10.5194/acp-22-5725-2022, 2022.

van Pinxteren, M., Zeppenfeld, S., Fomba, K. W., Triesch, N., Frka, S., and Herrmann, H.: Amino acids, carbohydrates, and lipids in the tropical oligotrophic Atlantic Ocean: sea-to-air transfer and atmospheric in situ formation, Atmospheric Chemistry and Physics, 23, 6571–6590, https://doi.org/10.5194/acp-23-6571-2023, 2023.

Platt, S. M., Hov, Ø., Berg, T., Breivik, K., Eckhardt, S., Eleftheriadis, K., Evangeliou, N., Fiebig, M., Fisher, R., Hansen, G., Hansson, H.-C., Heintzenberg, J., Hermansen, O., Heslin-Rees, D., Holmén, K., Hudson, S., Kallenborn, R., Krejci, R., Krognes, T., Larssen, S., Lowry, D., Lund Myhre, C., Lunder, C., Nisbet, E., Nizzetto, P. B., Park, K.-T., Pedersen, C. A., Aspmo Pfaffhuber, K., Röckmann, T., Schmidbauer, N., Solberg, S., Stohl, A., Ström, J., Svendby, T., Tunved, P., Tørnkvist, K., van der Veen, C., Vratolis, S., Yoon, Y. J., Yttri, K. E., Zieger, P., Aas, W., and Tørseth, K.: Atmospheric composition in the European Arctic and 30 years of the Zeppelin Observatory, Ny-Ålesund, Atmospheric Chemistry and Physics, 22, 3321–3369, https://doi.org/10.5194/acp-22-3321-2022, 2022.

van de Poll, W. H., Maat, D. S., Fischer, P., Visser, R. J. W., Brussaard, C. P. D., and Buma, A. G. J.: Solar radiation and solar radiation driven cycles in warming and freshwater discharge control seasonal and inter-annual phytoplankton chlorophyll a and taxonomic composition in a high Arctic fjord (Kongsfjorden, Spitsbergen), Limnology and Oceanography, 66, 1221–1236, https://doi.org/10.1002/lno.11677, 2021.

Porter, G. C. E., Adams, M. P., Brooks, I. M., Ickes, L., Karlsson, L., Leck, C., Salter, M. E., Schmale, J., Siegel, K., Sikora, S. N. F., Tarn, M. D., Vüllers, J., Wernli, H., Zieger, P., Zinke, J., and Murray, B. J.: Highly Active Ice-Nucleating Particles at the Summer North Pole, Journal of Geophysical Research: Atmospheres, 127, e2021JD036059, https://doi.org/10.1029/2021JD036059, 2022.

Quinn, P. K., Collins, D. B., Grassian, V. H., Prather, K. A., and Bates, T. S.: Chemistry and Related Properties of Freshly Emitted Sea Spray Aerosol, Chemical Reviews, 115, 4383–4399, https://doi.org/10.1021/cr500713g, 2015.

Ramasamy, K. P., Mahawar, L., Rajasabapathy, R., Rajeshwari, K., Miceli, C., and Pucciarelli, S.: Comprehensive insights on environmental adaptation strategies in Antarctic bacteria and biotechnological applications of cold adapted molecules, Front. Microbiol., 14, https://doi.org/10.3389/fmicb.2023.1197797, 2023.

Rinaldi, M., Decesari, S., Carbone, C., Finessi, E., Fuzzi, S., Ceburnis, D., O'Dowd, C. D., Sciare, J., Burrows, J. P., Vrekoussis, M., Ervens, B., Tsigaridis, K., and Facchini, M. C.: Evidence of a natural marine source of oxalic acid and a possible link to glyoxal, Journal of Geophysical Research: Atmospheres, 116, https://doi.org/10.1029/2011JD015659, 2011.

Robinson, T.-B., Stolle, C., and Wurl, O.: Depth is relative: the importance of depth for transparent exopolymer particles in the near-surface environment, Ocean Science, 15, 1653–1666, https://doi.org/10.5194/os-15-1653-2019, 2019a.

Robinson, T.-B., Wurl, O., Bahlmann, E., Jürgens, K., and Stolle, C.: Rising bubbles enhance the gelatinous nature of the air–sea interface, Limnology and Oceanography, 64, 2358–2372, https://doi.org/10.1002/lno.11188, 2019b.

Rocchi, A., von Jackowski, A., Welti, A., Li, G., Kanji, Z. A., Povazhnyy, V., Engel, A., Schmale, J., Nenes, A., Berdalet, E., Simó, R., and Dall'Osto, M.: Glucose Enhances Salinity-Driven Sea Spray Aerosol Production in Eastern Arctic Waters, Environ. Sci. Technol., 58, 8748–8759, https://doi.org/10.1021/acs.est.4c02826, 2024.

Russell, L. M., Hawkins, L. N., Frossard, A. A., Quinn, P. K., and Bates, T. S.: Carbohydrate-like composition of submicron atmospheric particles and their production from ocean bubble bursting, Proc. Natl. Acad. Sci. U.S.A., 107, 6652–6657, https://doi.org/10.1073/pnas.0908905107, 2010.

Sander, R., Keene, W. C., Pszenny, A. a. P., Arimoto, R., Ayers, G. P., Baboukas, E., Cainey, J. M., Crutzen, P. J., Duce, R. A., Hönninger, G., Huebert, B. J., Maenhaut, W., Mihalopoulos, N., Turekian, V. C., and Van Dingenen, R.: Inorganic bromine in the marine boundary layer: a critical review, Atmospheric Chemistry and Physics, 3, 1301–1336, https://doi.org/10.5194/acp-3-1301-2003, 2003.

Šantl-Temkiv, T., Gosewinkel, U., Starnawski, P., Lever, M., and Finster, K.: Aeolian dispersal of bacteria in southwest Greenland: their sources, abundance, diversity and physiological states, FEMS Microbiol Ecol, 94, https://doi.org/10.1093/femsec/fiy031, 2018.

Šantl-Temkiv, T., Amato, P., Casamayor, E. O., Lee, P. K. H., and Pointing, S. B.: Microbial ecology of the atmosphere, FEMS Microbiology Reviews, 46, fuac009, https://doi.org/10.1093/femsre/fuac009, 2022.

Schartau, M., Engel, A., Schröter, J., Thoms, S., Völker, C., and Wolf-Gladrow, D.: Modelling carbon overconsumption and the formation of extracellular particulate organic carbon, Biogeosciences, 4, 433–454, https://doi.org/10.5194/bg-4-433-2007, 2007.

Schill, S. R., Burrows, S. M., Hasenecz, E. S., Stone, E. A., and Bertram, T. H.: The Impact of Divalent Cations on the Enrichment of Soluble Saccharides in Primary Sea Spray Aerosol, Atmosphere, 9, 476, https://doi.org/10.3390/atmos9120476, 2018.

Schmale, J., Zieger, P., and Ekman, A. M. L.: Aerosols in current and future Arctic climate, Nature Climate Change, 11, 95–105, https://doi.org/10.1038/s41558-020-00969-5, 2021.

Schmale, J., Sharma, S., Decesari, S., Pernov, J., Massling, A., Hansson, H.-C., von Salzen, K., Skov, H., Andrews, E., Quinn, P. K., Upchurch, L. M., Eleftheriadis, K., Traversi, R., Gilardoni, S., Mazzola, M., Laing, J., and Hopke, P.: Pan-Arctic seasonal cycles and long-term trends of aerosol properties from 10 observatories, Atmospheric Chemistry and Physics, 22, 3067–3096, https://doi.org/10.5194/acp-22-3067-2022, 2022.

Sharma, S., Barrie, L. a., Magnusson, E., Brattström, G., Leaitch, W. r., Steffen, A., and Landsberger, S.: A Factor and Trends Analysis of Multidecadal Lower Tropospheric Observations of Arctic Aerosol Composition, Black Carbon, Ozone, and Mercury at Alert, Canada, Journal of Geophysical Research: Atmospheres, 124, 14133–14161, https://doi.org/10.1029/2019JD030844, 2019.

Shestakova, A., Chechin, D., Lüpkes, C., Hartmann, J., and Maturilli, M.: Foehn effect during easterly flow over Svalbard, https://doi.org/10.5194/acp-2021-478, 2021.

Simon, D. J., Hartmann, J., Schaefer, J., Zeppenfeld, S., Lüpkes, C., Hartmann, M., Wetzel, B., Heinold, B., Jurányi, Z., Schulz, A., Köhler, L., Jörss, A.-M., Herber, A., Henning, S., Pöhlker, M. L., Roberts, G. C., and Stratmann, F.: Turbulent aerosol fluxes from airborne measurements over the Arctic Ocean, *Geophys. Res. Lett.*, 52, e2025GL117094, https://doi.org/10.1029/2025GL117094, 2025

Sinreich, R., Coburn, S., Dix, B., and Volkamer, R.: Ship-based detection of glyoxal over the remote tropical Pacific Ocean, Atmospheric Chemistry and Physics, 10, 11359–11371, https://doi.org/10.5194/acp-10-11359-2010, 2010.

Sorooshian, A., Lu, M.-L., Brechtel, F. J., Jonsson, H., Feingold, G., Flagan, R. C., and Seinfeld, J. H.: On the Source of Organic Acid Aerosol Layers above Clouds, Environ. Sci. Technol., 41, 4647–4654, https://doi.org/10.1021/es0630442, 2007.

Stein, A. F., Draxler, R. R., Rolph, G. D., Stunder, B. J. B., Cohen, M. D., and Ngan, F.: NOAA's HYSPLIT Atmospheric Transport and Dispersion Modeling System, Bull. Amer. Meteor. Soc., 96, 2059–2077, https://doi.org/10.1175/BAMS-D-14-00110.1, 2015.

Struthers, H., Ekman, A. M. L., Glantz, P., Iversen, T., Kirkevåg, A., Mårtensson, E. M., Seland, Ø., and Nilsson, E. D.: The effect of sea ice loss on sea salt aerosol concentrations and the radiative balance in the Arctic, Atmospheric Chemistry and Physics, 11, 3459–3477, https://doi.org/10.5194/acp-11-3459-2011, 2011.

Su, B., Bi, X., Zhang, Z., Liang, Y., Song, C., Wang, T., Hu, Y., Li, L., Zhou, Z., Yan, J., Wang, X., and Zhang, G.: Enrichment of calcium in sea spray aerosol: insights from bulk measurements and individual particle analysis during the R/V *Xuelong* cruise in the summertime in Ross Sea, Antarctica, Atmospheric Chemistry and Physics, 23, 10697–10711, https://doi.org/10.5194/acp-23-10697-2023, 2023.

Theodosi, C., Im, U., Bougiatioti, A., Zarmpas, P., Yenigun, O., and Mihalopoulos, N.: Aerosol chemical composition over Istanbul, Science of The Total Environment, 408, 2482–2491, https://doi.org/10.1016/j.scitotenv.2010.02.039, 2010.

Thyng, K., Greene, C. A., Hetland, R. D., Zimmerle, H. M., and DiMarco, S.: True colors of oceanography: Guidelines for effective and accurate colormap selection, Oceanography, 3, https://doi.org/10.5670/oceanog.2016.66, 2016.

Tilgner, A. and Herrmann, H.: Radical-driven carbonyl-to-acid conversion and acid degradation in tropospheric aqueous systems studied by CAPRAM, Atmospheric Environment, 44, 5415–5422, https://doi.org/10.1016/j.atmosenv.2010.07.050, 2010.

Tørseth, K., Aas, W., Breivik, K., Fjæraa, A. M., Fiebig, M., Hjellbrekke, A. G., Lund Myhre, C., Solberg, S., and Yttri, K. E.: Introduction to the European Monitoring and Evaluation Programme (EMEP) and observed atmospheric composition change during 1972–2009, Atmospheric Chemistry and Physics, 12, 5447–5481, https://doi.org/10.5194/acp-12-5447-2012, 2012.

Trainic, M., Koren, I., Sharoni, S., Frada, M., Segev, L., Rudich, Y., and Vardi, A.: Infection Dynamics of a Bloom-Forming Alga and Its Virus Determine Airborne Coccolith Emission from Seawater, iScience, 6, 327–335, https://doi.org/10.1016/j.isci.2018.07.017, 2018.

Triesch, N., van Pinxteren, M., Engel, A., and Herrmann, H.: Concerted measurements of free amino acids at the Cabo Verde islands: high enrichments in submicron sea spray aerosol particles and cloud droplets, Atmospheric Chemistry and Physics, 21, 163–181, https://doi.org/10.5194/acp-21-163-2021, 2021.

Turekian, V. C., Macko, S. A., and Keene, W. C.: Concentrations, isotopic compositions, and sources of size-resolved, particulate organic carbon and oxalate in near-surface marine air at Bermuda during spring, Journal of Geophysical Research: Atmospheres, 108, https://doi.org/10.1029/2002JD002053, 2003.

Veron, F.: Ocean Spray, Annual Review of Fluid Mechanics, 47, 507–538, https://doi.org/10.1146/annurev-fluid-010814-014651, 2015.

Vihtakari, M.: PlotSvalbard: PlotSvalbard-Plot research data from Svalbard on maps, R package version 0.9 2, 2020.

Warneck, P.: In-cloud chemistry opens pathway to the formation of oxalic acid in the marine atmosphere, Atmospheric Environment, 37, 2423–2427, https://doi.org/10.1016/S1352-2310(03)00136-5, 2003.

Wendisch, M., Brückner, M., Burrows, J. P., Crewell, S., Dethloff, K., Ebell, K., Lüpkes, C., Macke, A., Notholt, J., and Quaas, J.: Understanding causes and effects of rapid warming in the Arctic, Eos, 98, 2017.

Wendisch, M., Brückner, M., Crewell, S., Ehrlich, A., Notholt, J., Lüpkes, C., Macke, A., Burrows, J. P., Rinke, A., Quaas, J., Maturilli, M., Schemann, V., Shupe, M. D., Akansu, E. F., Barrientos-Velasco, C., Bärfuss, K., Blechschmidt, A.-M., Block, K., Bougoudis, I., Bozem, H., Böckmann, C., Bracher, A., Bresson, H., Bretschneider, L., Buschmann, M., Chechin, D. G., Chylik, J., Dahlke, S., Deneke, H., Dethloff, K., Donth, T., Dorn, W., Dupuy, R., Ebell, K., Egerer, U., Engelmann, R., Eppers, O., Gerdes, R., Gierens, R., Gorodetskaya, I. V., Gottschalk, M., Griesche, H., Gryanik, V. M., Handorf, D., Harm-Altstädter, B., Hartmann, J., Hartmann, M., Heinold, B., Herber, A., Herrmann, H., Heygster, G., Höschel, I., Hofmann, Z., Hölemann, J., Hünerbein, A., Jafariserajehlou, S., Jäkel, E., Jacobi, C., Janout, M., Jansen, F., Jourdan, O., Jurányi, Z., Kalesse-Los, H., Kanzow, T., Käthner, R., Kliesch, L. L., Klingebiel, M., Knudsen, E. M., Kovács, T., Körtke, W., Krampe, D., Kretzschmar, J., Kreyling, D., Kulla, B., Kunkel, D., Lampert, A., Lauer, M., Lelli, L., Lerber, A. von, Linke, O., Löhnert, U., Lonardi, M., Losa, S. N., Losch, M., Maahn, M., Mech, M., Mei, L., Mertes, S., Metzner, E., Mewes, D., Michaelis, J., Mioche, G., Moser, M., Nakoudi, K., Neggers, R., Neuber, R., Nomokonova, T., Oelker, J., Papakonstantinou-Presvelou, I., et al.: Atmospheric and Surface Processes, and Feedback Mechanisms Determining Arctic Amplification: A Review of First Results and Prospects of the (AC)3 Project, Bulletin of the American Meteorological Society, 104, E208–E242, https://doi.org/10.1175/BAMS-D-21-0218.1, 2023.

White, W. H.: Chemical markers for sea salt in IMPROVE aerosol data, Atmospheric Environment, 42, 261–274, https://doi.org/10.1016/j.atmosenv.2007.09.040, 2008.

Wickham, H.: Reshaping Data with the reshape Package, Journal of Statistical Software, 21, 1–20, 2007.

Wickham, H.: ggplot2: Elegant Graphics for Data Analysis, Springer-Verlag New York, https://doi.org/10.1007/978-3-319-24277-4_2, 2016.

Wickham, H., François, R., Henry, L., Müller, K., and Vaughan, D.: dplyr: A Grammar of Data Manipulation, R package version 1.1.4, 2023a.

Wickham, H., Pedersen, T. L., and Seidel, D.: scales: Scale Functions for Visualization, R package version 1.3.0, 2023b.

Wietz, M., Engel, A., Ramondenc, S., Niwano, M., von Appen, W.-J., Priest, T., von Jackowski, A., Metfies, K., Bienhold, C., and Boetius, A.: The Arctic summer microbiome across Fram Strait: Depth, longitude, and substrate concentrations structure microbial diversity in the euphotic zone, Environmental Microbiology, 26, e16568, https://doi.org/10.1111/1462-2920.16568, 2024.

Wietz, M., van Pinxteren, M., Freese, H. M., Sproer, C., and Zeppenfeld, S.: Seasonal connectivity of microbes and carbohydrates between ocean, atmosphere, and cryosphere in Kongsfjorden (Svalbard, Arctic Ocean), preprint, https://doi.org/10.64898/2025.12.01.691664, uploaded on 2 December 2025.

Willis, M. D., Leaitch, W. R., and Abbatt, J. P. D.: Processes Controlling the Composition and Abundance of Arctic Aerosol, Reviews of Geophysics, 56, 621–671, https://doi.org/10.1029/2018RG000602, 2018.

Wong, J. P. S., Tsagkaraki, M., Tsiodra, I., Mihalopoulos, N., Violaki, K., Kanakidou, M., Sciare, J., Nenes, A., and Weber, R. J.: Effects of Atmospheric Processing on the Oxidative Potential of Biomass Burning Organic Aerosols, Environ. Sci. Technol., 53, 6747–6756, https://doi.org/10.1021/acs.est.9b01034, 2019.

Wurl, O. and Holmes, M.: The gelatinous nature of the sea-surface microlayer, Marine Chemistry, 110, 89–97, https://doi.org/10.1016/j.marchem.2008.02.009, 2008.

Xu, W., Ovadnevaite, J., Fossum, K. N., Lin, C., Huang, R.-J., Ceburnis, D., and O'Dowd, C.: Sea spray as an obscured source for marine cloud nuclei, Nat. Geosci., 15, 282–286, https://doi.org/10.1038/s41561-022-00917-2, 2022.

Yang, C., Zhou, S., Zhang, C., Yu, M., Cao, F., and Zhang, Y.: Atmospheric Chemistry of Oxalate: Insight Into the Role of Relative Humidity and Aerosol Acidity From High-Resolution Observation, Journal of Geophysical Research: Atmospheres, 127, e2021JD035364, https://doi.org/10.1029/2021JD035364, 2022.

Yttri, K. E., Bäcklund, A., Conen, F., Eckhardt, S., Evangeliou, N., Fiebig, M., Kasper-Giebl, A., Gold, A., Gundersen, H., Myhre, C. L., Platt, S. M., Simpson, D., Surratt, J. D., Szidat, S., Rauber, M., Tørseth, K., Ytre-Eide, M. A., Zhang, Z., and Aas, W.: Composition and sources of carbonaceous aerosol in the European Arctic at Zeppelin Observatory, Svalbard (2017 to 2020), Atmospheric Chemistry and Physics, 24, 2731–2758, https://doi.org/10.5194/acp-24-2731-2024, 2024.

Yu, H., Kaufman, Y. J., Chin, M., Feingold, G., Remer, L. A., Anderson, T. L., Balkanski, Y., Bellouin, N., Boucher, O., Christopher, S., DeCola, P., Kahn, R., Koch, D., Loeb, N., Reddy, M. S., Schulz, M., Takemura, T., and Zhou, M.: A review of measurement-based assessments of the aerosol direct radiative effect and forcing, Atmospheric Chemistry and Physics, 6, 613–666, https://doi.org/10.5194/acp-6-613-2006, 2006.

Zäncker, B., Cunliffe, M., and Engel, A.: Eukaryotic community composition in the sea surface microlayer across an east–west transect in the Mediterranean Sea, Biogeosciences, 18, 2107–2118, https://doi.org/10.5194/bg-18-2107-2021, 2021.

Zeppenfeld, S. and Schmidt, L.: Dissolved and particulate carbohydrates and inorganic ions in the sea surface microlayer and bulk water of Kongsfjorden (Autumn 2021/Spring 2022), https://doi.org/10.1594/PANGAEA.982606, 2025.

Zeppenfeld, S., van Pinxteren, M., Engel, A., and Herrmann, H.: A protocol for quantifying mono- and polysaccharides in seawater and related saline matrices by electro-dialysis (ED) – combined with HPAEC-PAD, Ocean Science, 16, 817–830, https://doi.org/10.5194/os-16-817-2020, 2020.

Zeppenfeld, S., van Pinxteren, M., van Pinxteren, D., Wex, H., Berdalet, E., Vaqué, D., Dall'Osto, M., and Herrmann, H.: Aerosol Marine Primary Carbohydrates and Atmospheric Transformation in the Western Antarctic Peninsula, ACS Earth Space Chem., 5, 1032–1047, https://doi.org/10.1021/acsearthspacechem.0c00351, 2021.

Zeppenfeld, S., van Pinxteren, M., Hartmann, M., Zeising, M., Bracher, A., and Herrmann, H.: Marine carbohydrates in Arctic aerosol particles and fog – diversity of oceanic sources and atmospheric transformations, Atmospheric Chemistry and Physics, 23, 15561–15587, https://doi.org/10.5194/acp-23-15561-2023, 2023.

Zeppenfeld, S., Schaefer, J., van Pinxteren, M., and Schmidt, L.: Marine combined carbohydrates and inorganic ions in atmospheric total suspended particles across altitudes in the lower troposphere of Ny-Ålesund, Svalbard, https://doi.org/10.1594/PANGAEA.982703, 2025.

Zhou, S., Gonzalez, L., Leithead, A., Finewax, Z., Thalman, R., Vlasenko, A., Vagle, S., Miller, L. A., Li, S.-M., Bureekul, S., Furutani, H., Uematsu, M., Volkamer, R., and Abbatt, J.: Formation of gas-phase carbonyls from heterogeneous oxidation of polyunsaturated fatty acids at the air–water interface and of the sea surface microlayer, Atmospheric Chemistry and Physics, 14, 1371–1384, https://doi.org/10.5194/acp-14-1371-2014, 2014.

Zhu, B., Sun-Waterhouse, D., and You, L.: Insights into the mechanisms underlying the degradation of xylooligosaccharides in UV/H2O2 system, Carbohydrate Polymers, 317, 121091, https://doi.org/10.1016/j.carbpol.2023.121091, 2023.

Zhu, Y.-S., Connolly, A., Guyon, A., and FitzGerald, R. J.: Solubilisation of calcium and magnesium from the marine red algae Lithothamnion calcareum, International Journal of Food Science and Technology, 49, 1600–1606, https://doi.org/10.1111/ijfs.12459, 2014.